DHBW Ravensburg
Duale Hochschule
Baden-Württemberg

HYPER
(HYdrogen Powered Electric Regional aircraft)

Bachelor's Program

- 4th Semester Aerospace Engineering -

Jonna Bleeker

Lena Hennige

Niclas Neufeld

Jonas Schaur

Lucas Weser

Julius Wildeboer

21st of July 2024

DHBW Ravensburg Campus Friedrichshafen

Table of Contents

Nomenclature

Symbols

$\Lambda_{0.25}$	Sweep Angle	°
AR	Aspect Ratio	-
a	annuity factor	-
α	Angle of attack	*deg*
α_0	Zero-lift angle of attack	*deg*
b	Wingspan	*m*
B	Maintenance cost Burden	-
BE	Block Energy	-
C_D	Drag coefficient	-
$C_{D,0}$	Zero-lift drag coefficient	-
C_L	Lift coefficient	-
$C_{L,md}$	Lift coefficient for minimum drag	-
c	Cost	$
CC	Crew Complement	-
cl	Chord length	*m*
D	Drag	*N*
DP	Depreciation Period	a
e_o	Wingspan efficiency	-
E	Energy	kWh
η	efficiency	%
η_{ult}	Ultimate Load Factor	-
f_{ins}	insurance rate	-
f_{misc}	miscellanous factor	-
f_{RV}	Residual Value factor	-
f	factor	-
F_{nose}	Load on Nose Wheel	N
FT	Flight Timeh	
g	acceleration due to gravity	m/s^2
H_{cg}	Distance COP to ground	m
h	Height	m
IR	Interest Rate	%
k	cost factor	-
K_L	Emperical LG Value	-
K_{LG}	Emperical LG Value	-
K_{ret}	Retractable LG Value	-

K_ρ	Wing Density factor	-
L	Lift	N
λ	Taper Ratio	-
LR	Labor Rate	%
M	Mach number	$Mach$
m	mass	kg
MAC	Mean Aerodynamic Chord	m
MTOW	Max. Take-Off Weight	kg
MZFW	Max. Zero-Fuel Weight	kg
n_g	Gravimetric density	%
n_ν	Volumetric density	MJ/l
n	Number	-
NRC	Non Recurring Costs	$
OEW	Operational Empty Weight	kg
$\text{OT}_{p.a}$	Yearly Operational Flight Time	h
φ	Wingsweep	$^\circ$
PM	Profit Margin	%
$\text{POT}_{p.a}$	Average Stage Length	km
P	Price	$
RC	Recurring Costs	$
ρ_{mat}	Density of Construction material	kg/m^3
R	Range	km
R_r	Turn Radius	m
S	Area	m^2
S	Salary	$
t/c	Thickness to chord ratio	%
TW	Track Width	m
T	Thrust	t
V	Volume	m^3
V_{taxi}	Taxi Speed	m/s
v	cruise speed	km/h
W_L	Landing Gear Weight	kg
YFC	Yearly Flight Cycles	-

Indices

AC	Aircraft
ATC	Air Traffic Control
avg	Average

BAT	Battery
box	Boxwing
cmd	Command
eng	engine
FA	Flight Attendants
FC	Flight Crew
FC	Fuel Cell
fuse	Fuselage
HT	Horizontal Tail
i	Aircraft components & systems
min	minimum
opt	Optimal
ref	Reference
r	Wingroot
SL	Sea Level
tot	Total
t	Wingtip
V	V-tail
W	Wing

Abbreviations

APU	Auxiliary Power Unit
BLI	Boundary Layer Ingestion
BoP	Balance of Plant
BWA	Boxwing Aircraft
BWB	Blended Wing Body
CG	Center of gravity
DOC	Direct Operating Cost
EASA	European Aviation Safety Agency
EIS	Entry Into Service
FC	Fuel Cell
FW	Flying Wing
HT-PEMFC	High Temperature Proton Exchange Membrane Fuel Cell
HYPER	HYdrogen Powered Electric Regional aircraft
IEA	International Energy Agency
LG	Landing Gear
LH2	liquid hydrogen
LI-air	Lithium-air

LI-S	Lithium-Sulfur
LIB	Lithium-Ion Battery
MLW	Maximum Landing Weight
NP	Neutral point
PAX	Number of passengers
SAF	Sustainable Aviation Fuel
SiPO	Single Pilot Operations
SOFC	Solid Oxid Fuel Cell
TRL	Technology Readiness Level
UAV	Unmanned Aerial Vehicle

ABSTRACT

This report presents the innovative design and feasibility study of the HYdrogen Powered Electric Regional aircraft (HYPER), developed for the DLR Design Challenge 2024. The HYPER aircraft is poised to transform regional air travel by 2050, featuring a zero-emission propulsion system. Its futuristic boxwing configuration enhances aerodynamic efficiency and operational performance. The aircraft's capability for steep takeoffs and landings increases its adaptability to diverse airport environments, contributing to a reduction in noise pollution.
The technical specifications of HYPER include a maximum range of 1,250 km and a passenger capacity of up to 89 PAX. The design incorporates advanced aerodynamics, with a particular focus on the boxwing and tail geometry to ensure stability and controllability. The powertrain features boundary layer ingestion (BLI) technology, hydrogen fuel cells, and cutting-edge battery systems, which collectively contribute to an efficient and robust power system architecture.
A key objective of the HYPER project is to maximize both cost efficiency and sustainability. The report includes a comprehensive analysis of Direct Operating Costs (DOC), with estimates indicating a DOC of approximately 11 million $. Detailed assessments of energy consumption, maintenance, and operational costs highlight the potential for significant cost savings. HYPER's energy consumption is notably efficient, ranging from 280.4- to 389.5 kJ/PAX/km, demonstrating superior performance compared to the reference aircraft, the Dash 8 Q400, in both DOC and energy consumption metrics.

ZUSAMMENFASSUNG

Dieser Bericht präsentiert das innovative Design und die Machbarkeitsstudie des HYdrogen Powered Electric Regional Aircraft (HYPER), entwickelt im Rahmen der DLR Design Challenge 2024. Das HYPER-Flugzeug ist darauf ausgelegt, den regionalen Luftverkehr bis 2050 zu revolutionieren, indem es ein emissionsfreies Antriebssystem verwendet. Die futuristische Boxwing-Konfiguration verbessert die aerodynamische Effizienz und die Betriebsleistung. Die Fähigkeit des Flugzeugs zu steilen Starts und Landungen erhöht seine Anpassungsfähigkeit an verschiedene Flughafenumgebungen und trägt zur Reduzierung der Lärmbelastung bei.
Die technischen Spezifikationen des HYPER umfassen eine maximale Reichweite von 1.250 km und eine Passagierkapazität von bis zu 89 PAX. Das Design integriert fortschrittliche Aerodynamik, insbesondere mit Fokus auf die Boxwing- und Heckgeometrie, um Stabilität und Steuerbarkeit zu gewährleisten. Der Antriebsstrang nutzt die Technologie der Boundary Layer Ingestion (BLI), Wasserstoff-Brennstoffzellen und hochmoderne Batteriesysteme, die gemeinsam zu einer effizienten und robusten Antriebsarchitektur beitragen.
Ein zentrales Ziel des HYPER-Projekts ist es, sowohl die Kosten-effizienz als auch die Nachhaltigkeit zu maximieren. Der Bericht enthält eine umfassende Analyse der Direkten Betriebskosten (DOC), wobei sich diese auf etwa 11 Millionen $ hinweisen. Detaillierte Bewertungen des Energieverbrauchs sowie der Wartungs- und Betriebskosten zeigen das Potenzial für erhebliche Kosteneinsparungen auf. Der Energieverbrauch von HYPER ist bemerkenswert effizient und liegt im Bereich von 280,4- bis 389,5 kJ/PAX/km, was eine überlegene Leistung im Vergleich zum Referenzflugzeug, dem Dash 8 Q400, sowohl in Bezug auf die DOC als auch auf die Energieverbrauchsmesswerte demonstriert.

1. INTRODUCTION

As the global demand for air travel continues to rise, the aerospace industry faces increasing pressure to address its environmental impact. Therefore, political incentives are set into motion, such as the EU's European Green Deal aiming for net-zero emissions by 2050 [1]. To achieve these ambitious goals, new concepts have to be developed with the objective to reduce environmental impact while keeping air transport affordable. Additional issues such as noise pollution have to be adressed as well. To account for this need for change, the assignment in this year's DLR Design Challenge consists of the development of a short-haul aircraft tailored to a given regional network focusing on Hamburg airport. With the objective of optimizing the energy consumption and direct operating costs (DOC) of the developed aircraft, different sustainable energy sources as well as aerodynamic concepts are investigated and compared.

The results of this process are presented in this paper, in the form of the development of an aircraft called HYPER (HYdrogen Powered Electric Regional aircraft). This aircraft has a maximum passenger capacity of 89 PAX and a maximum range of 1250 km. HYPER is a fully electric concept using hydrogen as main energy source in combination with batteries to minimize environmental impact. For optimized aerodynamic efficiency and therefore energy consumption, the aircraft makes use of a boxwing configuration. The propulsion system is based on electric motors and propellers. HYPER's entry into service (EIS) is planned for 2050.

2. METHODOLOGY

For the general design process of HYPER, the methodology presented in "Aircraft Design - A Systems Engineering Approach" by Mahammad H. Sadraey [2] is applied. This process consists of several design phases beginning with the analysis of requirements and their prioritization. These requirements are the input for the conceptual design phase, where the configuration of the aircraft is selected as well as its energy source. These two steps are presented in Chapter 3. After the concept is selected, the preliminary design phase is performed. Its output consists of the wing loading and the power loading of the aircraft from which the reference area of the wings and the required power for thrust can be deduced. The exact process and its input parameters are presented in chapter 4. Using this output, the components of the aircraft are designed in detail and the resulting system is evaluated. Since the complete design of the aircraft has an influence on the values used as input for the preliminary design phase, this process is iterative. The entire procedure is presented in Figure 1.

3. CONCEPT SELECTION

The initial concept selection process involved a comprehensive research study that examined not only currently existing concepts but also experimental studies in this area. This extensive review included a wide range of literature and publications. The main aspects of the research explored configurational and aerodynamic design, alongside propulsion systems and potential energy sources.

The final selection of concepts is based on the specific requirements outlined in the competition assignment. This approach ensures that the chosen concepts are innovative whilst also aligned with the assignment's goals and constraints. Moreover, determining own requirements allows for a holistic approach to the task and ensures the establishment of a high standard.

3.1. Requirements

Resulting from this year's DLR Design Challenge assignment, the identified requirements and their satisfaction criteria are presented in Chapter 9. Additional self-determined requirements include the improvement of ground administration at airports, the reduction of noise pollution, and the relinquishment of the use of SAF. While SAF is recognized as a necessary step toward climate-neutral air traffic, it is also acknowledged that its fundamental reliance on a combustion process naturally results in the emission of greenhouse gases.

Maximum runway length	<1510 m
Sink angle below 1000 m	>5,5°
Ascending angle below 1000 m	4,0°
Average passenger weight (incl. luggage)	95 kg
Entry-Into-Service	2050
Diversion Range	250 km

TAB 1. Design specifications

3.2. Network Specifications

This section provides a brief discussion of the network specifications. According to the task requirements, this network is to serve 15 regional European airports, with Hamburg as the central hub. To limit the number of possible flights, slot restrictions have been implemented for Hamburg Airport. A minimum of 142 and a maximum of 276 slots can be utilized. The network is analyzed to determine the maximum passenger capacity needed to optimally cover the given network.

3.2.1. Determination of the maximum passenger capacity

The maximum passenger capacity for HYPER is determined based on the route network requirements. Initially, the minimum and maximum passenger capacities are established using the given slot specifications from Hamburg Airport described in Section 3.2. This figure is determined by summing the total weekly demand from all airports and then doubling the result, because the task

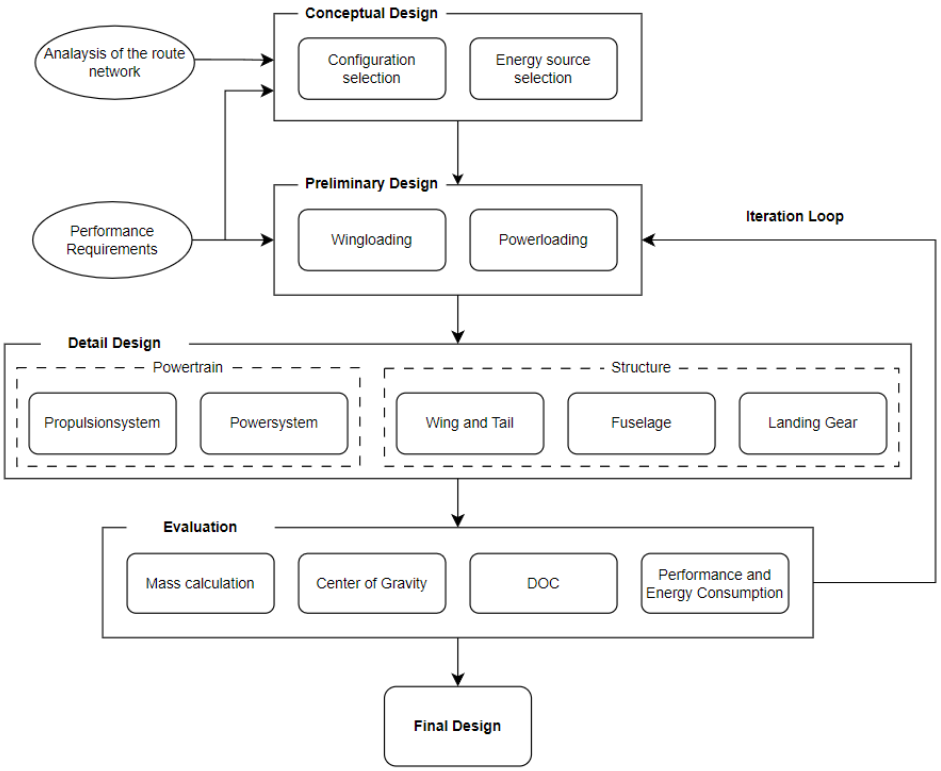

FIG 1. Flowchart of the design steps

states that the demand is specified per direction, and both directions must be covered. Flights that do not transit through Hamburg (GOT to UME and GOT to VBY) are subtracted from the initial total. Consequently, the number of passengers traveling via Hamburg is determined to be 15,886 PAX. Using this figure, along with the slot allocations, which are divided by the determined number of passengers traveling via Hamburg, a minimum and maximum passenger capacity is calculated. The determined range lies between 58 PAX and 112 PAX.
To determine the optimal value within this range that allows the highest number of flights at maximum passenger capacity, each all the options within the specified range are evaluated. This is done by dividing each passenger number by the number of passengers that need to be handled at each individual airport. The resulting figures are then rounded down to determine the number of flights at maximum passenger capacity and rounded up to determine the necessary number of flights. By summing the results of both rounding processes and calculating the difference, the number of flights is identified, where the capacity of the aircraft is not fully utilized. Such flights are subsequently referred to as underbooked flights.
This analysis allows for determining the most efficient passenger number per aircraft to minimize underbooked flights and thus maximize the profitability and economic efficieny of the missions covered by HYPER.
The optimal value is found to be 89 passengers, resulting in only 26 underbooked flights per week (13 per direction). Compared to other passenger numbers, this choice can reduce up to two underbooked flights per direction.

3.2.2. Range Determination

According to the given Network, the maximum range of the designed aircraft needs to be between 894 km for a flight from Edinburgh to Hamburg and 1480 km for a nonstop flight from Bari to Hamburg. If the maximum range is chosen to be the latter, all flightmissions can be completed without stopovers for refueling. However, because of the specific characteristics of HYPER, its maximum range is set to be 1250 km. The reasoning behind this decision is explained in further detail when exploring the aircrafts power train in Section 5.1.4.

3.3. Energy Source Selection

In order to achieve the goals of flight path 2050 [1] and to give flying a more sustainable future, alternatives to the classic kerosene-based power system need to be found. There are different kinds of energy sources that could be imagined for the demanded aircraft. All options have to be compared regarding emissions, coasts, weight and other key challenges. The proposed and most suitable energy sources for this application are hydrogen, batteries and SAF as stated in the competition's assignment. However, additional fewer common options such as ammonia were taken into consideration as well.

The most convenient way of switching to an alternate energy source would be choosing one that does not require any changes to the airport infrastructure or aircraft. Kerosene-like sustainable aviation fuels would be the best option according to this reasoning [4]. The use of SAF could reduce CO_2 emissions by up to 80 %. Nevertheless, SAF is not a true zero solution as it directly causes

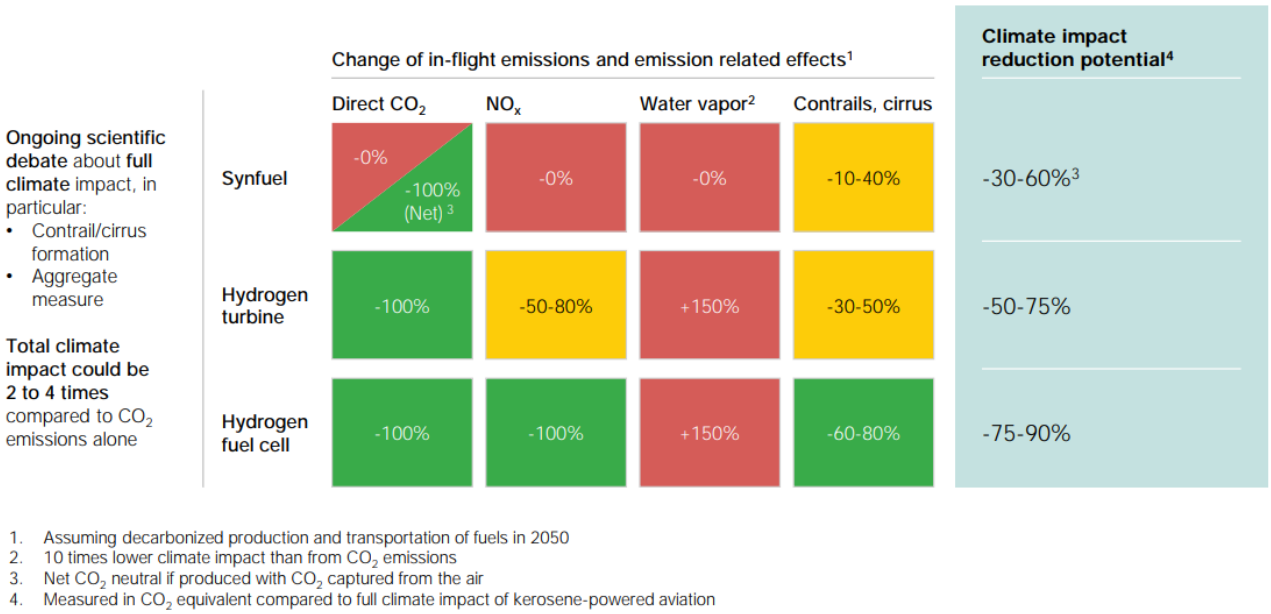

FIG 2. Emissions of different energy sources [3]

CO_2 and NO_x emissions and contrails as seen in Figure 2. In addition to that, it is hard to predict whether the demand for SAF could be covered in 2050 [5]. Given the need to make aviation truly sustainable, it was decided to explore innovative solutions and break away from existing paradigms, which led to the decision not to use SAF.

Another option is the usage of batteries as energy source. With this technology the flight itself would be very sustainable in regard to emissions, as there would be no CO_2, no NO_x and no contrails. This configuration would be quiet and simple with a high electric efficiency. However, for a true-zero solution the used electricity has to be produced in a sustainable manner. The key challenge of this type of electric propulsion is the weight of the batteries as they have a lower energy density than kerosene and do not lose weight during flight. This is a limiting factor for payload and range. There are different evaluations about the development of batteries regarding their energy densityand a variety of research projects. Today's lithium-ion batteries reach an energy density of up to 250 Wh/kg [6] [7]. Although the advancement of battery technology is promising, for flights up to 894 km the batteries are still too heavy as the only energy source, but can be used in combination with other energy sources [6].

An alternative or additional energy source could be hydrogen with two different options to generate thrust for the aircraft. Either hydrogen and oxygen are burned in a gas turbine engine to rotate a turbine which rotates a fan or a Fuel Cell converts hydrogen and oxygen into electricity which powers a motor that spins a propeller or ducted fan. Both options do not produce CO_2, but only water vapor emissions 2. Nevertheless one big difference is that for hydrogen combustion NO_x emissions are present while Hydrogen Fuel Cells have potential for a true zero solution and are more efficient than hydrogen combustion [6]. One key challenge when using hydrogen as aviation fuel is the storage as hydrogen has a higher gravimetric energy density but a lower volumetric energy density than kerosene [4].

To avoid the storage problem, ammonia could be considered as it is liquid at -33°C and can therefore be stored and transported in a more energy-saving manner in comparison to hydrogen. However, ammonia is toxic, environmentally hazardous and has a lower calorific value than hydrogen. Moreover, technologies other than direct combustion in a gas turbine with NO_x emissions are less mature, especially in terms of aviation [8] which is why this option is not investigated further.

Due to the advantages and disadvantages mentioned, a concept with Hydrogen Fuel Cells supported by batteries was chosen. HYPER is therefore a fully electric aircraft with electric propulsion and subsystems [6]. The identified key challenges of this concept are the weight of the power system and the volume of the hydrogen tank.

The main advantages are the low emissions and the high electrical efficiency. Compared to a conventional kerosene driven aircraft, an all electric aircraft can be 2-3 times more efficient [9].

Increased hydrogen applications and governmental support are likely to boost production of this low-emission fuel. The IEA projects that economies of scale could reduce the price of Hydrogen Fuel Cells by up to 75% and cut fueling station capital costs by 50% by 2030. Additionally, sustainable hydrogen production costs are expected to decrease by 30% due to falling renewable energy costs [10].

3.3.1. Emissions

As mentioned and seen in Figure 2 the selected configuration has no direct CO_2 and NO_x but only water vapour emissions. Therefore it has the potential of a climate impact reduction of up to 90% [3]. At lower altitudes, the water emissions from the Fuel Cells are less likely to form contrails compared to higher altitudes, which helps mitigate their contribution to global warming [5]. A flight altitude of 8000 m was chosen for HYPER to balance environmental impact and aerodynamic efficiency.
When discussing emissions, it is important to consider not only the emissions during flight but also those associated with the production of hydrogen and electricity.
To assess the sustainability and emissions of hydrogen, a color code classifies hydrogen based on its production method. Currently, 95% of hydrogen produced is "grey hydrogen," derived from splitting fossil fuels using electricity from fossil energy sources, resulting in significant CO_2 emissions. The only production method for fully climate-neutral hydrogen is "green hydrogen," produced through water electrolysis, which consumes a large amount of electrical energy [5]. It is expected that by 2050, most or all electricity will come from sustainable sources, significantly reducing or eliminating emissions [11] during the production of hydrogen.

3.3.2. Safety and Certification

When implementing new and unconventional concepts, the consideration of safety and certifiability becomes particularly relevant. Considering both hydrogen and batteries, special attention must be paid to fire hazards. Lithium batteries can present various risks, especially fire hazards due to heating, short circuits, overcharging, deep discharge, or fire spread [12]. Nevertheless, electric flying can be considered safe when batteries are properly stored, regularly maintained, and continuously temperature controlled. Although there are no specific studies on electric flying due to its rarity, examining the automotive industry — where similar battery technology is used — shows no increased incidents with electric vehicles compared to combustion engine vehicles [13].
Hydrogen has a higher auto-ignition temperature and diffuses quickly into the air, reducing the risk of ground-level accumulation. Unlike fossil fuels, a hydrogen spill doesn't pose a significant environmental hazard. However, its low minimum ignition energy and wider flammability range requires careful handling and robust safety measures like proper insulation [10].
To adapt CS-25 certification specifications for HYPER powered by Hydrogen Fuel Cells and batteries, several key updates are necessary. Regulations must address safe hydrogen storage and distribution, including the use of suitable materials and specific ventilation and cooling requirements. Energy management systems for batteries should prevent overcharging and overheating, and fire protection measures must be enhanced for both hydrogen and batteries.
Electrical systems regulations need to ensure redundancy and reliability, with specific requirements for power electronics integration. Control and monitoring systems should be expanded to include Hydrogen Fuel Cells and batteries, with necessary sensors for leak detection and fault monitoring.
Performance metrics and testing methods must be adjusted to reflect the characteristics of these new propulsion systems. Cabin safety regulations should account for the specific needs of hydrogen and battery systems, including updated evacuation procedures and safety equipment.
Maintenance and inspection requirements should include regular checks of hydrogen tanks, Fuel Cells, and batteries, with updated training for maintenance personnel.
Lastly, ground infrastructure regulations must ensure safe hydrogen refueling and handling procedures [14].
Given the pressing need for increased sustainability in aviation, it is anticipated that the certification standards for CS-25 will be adjusted by 2050. Many projects involving hydrogen-powered aircraft are targeting market entry by 2035 so it can be assumed that CS-25 was already significantly changed before the EIS.

3.4. Configuration Selection

In the final selection of configurations, three innovative designs were considered, each distinct from conventional aircraft designs. Special emphasis was placed on aerodynamic efficiency to reduce energy consumption. These parameters are directly aligned with this year's assignment goals of sustainability and minimizing direct operating costs.

- Blended Wing Body (BWB)
- Flying Wing (FW)
- Boxwing Aircraft (BWA)

Configurations such as FW or BWB have been extensively researched and discussed by global market leaders in the aircraft industry, demonstrating significant potential for the future. However, for the specified design requirements — short-range missions within a 1500 km radius and accommodating a limited passenger capacity of 89 — configurations like BWB and FW are less suitable. These designs excel with high passenger volumes where their high payload-to-empty-weight ratios become economically advantageous [15].

The BWA configuration is derived from the conventional tube-and-wing configuration. Instead of two wings, the BWA utilizes four wings, interconnected by extended winglets. The front wing is usually mounted at the bottom of the fuselage, while the rear wing is either attached to the top of the fuselage or integrated with the vertical tail [16]. The primary advantage of the BWA configuration lies in its reduced aerodynamic drag compared to conventional designs, resulting in higher lift-to-drag ratios. This reduction in drag is illustrated by the basic condition for minimal drag as depicted in Figure 3.
According to this principle, each drag component amounts for exact half of the total drag, leading to its overall minimization. Therefore, assuming each

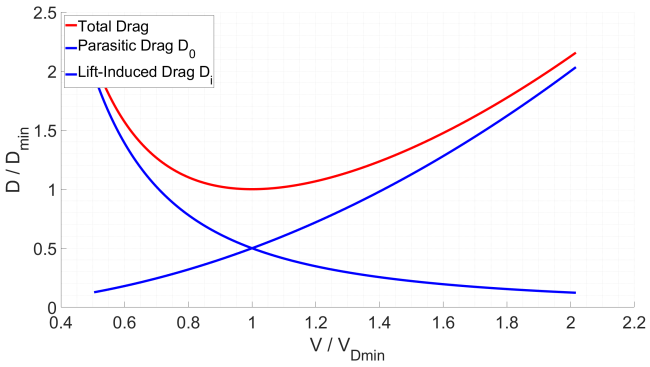

FIG 3. Drag over Velocity

pair of wings contributes equally to lift production, the Lift-to-Drag ratio is increased by approximately 33%.
Wake turbulence adversely affects airport efficiency by requiring increased separation between successive departing aircraft. The implementation of BWAs could potentially enhance overall airport efficiency by reducing these separation requirements through reduced vortex generation [17].
In terms of ground handling improvements, the structural characteristics of a BWA, detailed in Chapters 4 and 6, include an increased fuselage diameter that accommodates a twin-aisle configuration, as presented in Section 6.2. This facilitates quicker boarding and deboarding processes. The narrower central wing boxes of the BWA provide a continuous cargo bay throughout the fuselage, unlike conventional designs where larger wing central boxes divide the cargo area. The wing boxes of the BWA can be integrated beneath the cargo bay, thereby increasing volume and allowing for an optimized loading and unloading process with simultaneous operations through dual cargo doors.
Additional advantages include simplified qualification processes according to EASA's CS-25 standards, particularly when compared to BWB or FW concepts, due to the BWA's structural and operational similarities with conventional aircraft designs. Moreover, existing airport infrastructures would require minimal modification, due to the BWA's compatible fuselage design.

4. AERODYNAMICS

As outlined in Chapter 2, the design process transitions to the preliminary design phase following the selection of the concept. For this, aerodynamic calculations were conducted following the introduced methodology of Sadraey's "Aircraft Design: A Systems Engineering Approach" [2]. The aerodynamic design is result of the preliminary design phase, specifically of "Wing Area and Engine Sizing", subsequent to the initial weight estimation, which is primarily based on statistics. In this step, the wing reference area and engine power for propeller-driven propulsion systems are determined based solely on aircraft performance requirements and flight mechanics theories. This analytical approach ensures high reliability of the results, minimizing the risk of inaccuracies. The aircraft performance requirements utilized for sizing the aircraft in this phase include:

- stall speed V_s
- maximum speed V_{max}
- maximum rate of climb ROC_{max}
- take-off run S_{TO}
- ceiling h_c

These input parameters were selected according to the specified requirements or estimated using statistical values from various aircraft. Among these, the DHC-8-400, detailed in Chapter 7.1, served as a reference aircraft due to the similarity of its mission parameters to those of our study, providing a valuable benchmark for our estimations. From these requirements, the wing loading and power loading for the aircraft are calculated. These parameters are defined by Sadraey as follows [2]:

Wing Loading. Wing loading ($\frac{W}{S}$) is defined as ratio between the aircraft's weight and wing area. This parameter indicates how much load each unit area of the wing carries.

Power Loading. Power loading ($\frac{W}{P}$) is the ratio between the aircraft's weight and engine power. This parameter compares the aircraft's weight with its engine power and is specific to propeller-driven aircraft.

A given set of equations is derived for each parameter and sketched into a single plot, with power loading on the vertical axis and wing loading on the horizontal axis. This graph represents all variations of power loading concerning wing loading. The plotted curves intersect at several points, creating distinct regions. The acceptable area that meets all aircraft performance requirements is identified within these regions. A design point is then determined, providing the respective wing loading and power loading. The wing area and required power are calculated from the maximum take-off weight (MTOW). The resulting wing and power loading values are subsequently used in the iterative dimensioning process.

The optimal design point was selected based on the primary requirements of the challenge's assignment, which emphasizes low operating costs and minimal environmental impact. This approach results in a design point that minimizes engine power requirements, thereby meeting these critical criteria. The resulting plot is shown in Figure 4.

The region between the graphs of maximum speed and stall speed represents the acceptable area. Within this region, the smallest engine with the lowest power requirement corresponds to the lowest operating cost. Consequently, the highest point in this region is selected as

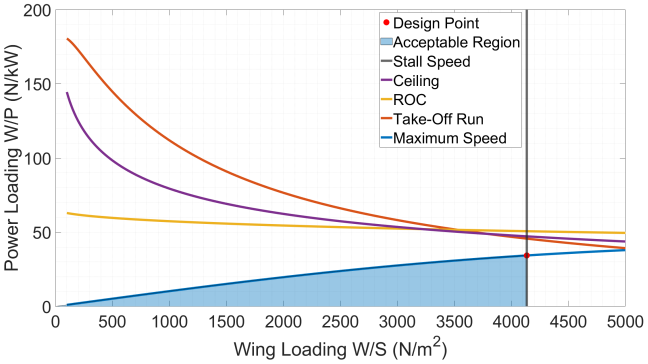

FIG 4. Matching Plot for HYPER

the design point. From this point, the wing loading and power loading are determined as follows:

$$\left(\frac{W}{P}\right)_d = 34.33\,\frac{N}{kW} \tag{1}$$

$$\left(\frac{W}{S}\right)_d = 4,134.38\,\frac{N}{m^2} \tag{2}$$

The preliminary wing area and engine power is calculated as follows:

$$P = \left(MTOW \cdot g \Big/ \left(\frac{W}{P}\right)_d\right) = 8,152.14\,\text{kW} \tag{3}$$

$$S = \left(MTOW \cdot g \Big/ \left(\frac{W}{S}\right)_d\right) = 67.70\,\text{m}^2 \tag{4}$$

4.1. Boxwing

For the dimensioning of the boxwing, the methodology given in "Boxwing Fundamentals" by D.Schiktanz and D. Scholz [18] is applied, where the boxwing is modeled using a reference wing. For this concept, a conventional wing is modeled following the methodology proposed by Sadraey [2] according to the values given by the design point estimation explained in the previous chapter. This wing is split up in two parts forming the forward and aft wing while maintaining the span of the reference wing. Their individual geometry is discussed in Section 5.2.

Regarding the overall configuration, an important parameter when dimensioning a box wing is the vertical distance between the wings. Because there are interference effects between the two components, that impact the induced drag negatively, the distance has to be as high as possible. This parameter can be expressed through the height to span ratio h/b. Studies have shown, that a height to span ratio greater than 0,2 increases the risk for fluttering of the wings [19]. Therefore, 0,2 is chosen as the ideal ratio. With a span of 25,5 m the distance between the wings is determined to be 5,1 m. To be able to achieve this distance between the wings, a negative horizontal stagger is chosen, where the aft wing is supported by the Tail. To provide enough structural stability, a V-Tail is chosen. The effects of the height to span ratio on the induced drag can be illustrated by the span efficiency e_0. The relation is shown in equation 5 [18].

$$e_{0,\,\text{box}} = e_{0,\,\text{ref}} \cdot \frac{0.44 + 2.219\frac{h}{b}}{0.44 + 0.9594\frac{h}{b}} \tag{5}$$

with a value of 0,85 for a conventional aircraft during cruise [20], the span efficiency of HYPER lies at 1,19.

4.2. Wing Geometry

To determine the geometry of the two wings, the influence of various parameters on the overall concept are investigated and defined. The Aspect Ratio AR of the wing has an influence on its induced drag as well as the wing lift curve slope. To optimize both parameters, a high Aspect Ratio is desired [2]. Since the boxwing consists of two wings there is a difference between the Aspect Ratio of the whole configuration and the individual wing. For this configuration, both wings have the same wingspan and half of the total wing area. This means that the individual Aspect Ratio is double of the one of the whole configuration. The Aspect Ratio of the configuration is chosen to be 9,6 according to the reference wing.

The Taper Ratio λ of a wing has an influence on the lift distribution along the span. Since the lift distribution of a boxwing aircraft differs from conventional wings, formulas for estimating the Taper Ratio such as formula 6 [21] yield unrealistic results. In this design phase, a Taper Ratio of 0,28 is chosen based on comparable aircraft.

$$\lambda_{\text{opt}} = 0.45 \cdot e^{-0.036\varphi} \tag{6}$$

The Wingsweep φ is chosen to be 25° for the forward and -25° for the aft wing. From an aerodynamic standpoint, Sweep is only needed at transsonic, supersonic, and hypersonic speeds. However, Sweep can be additionally used as a tool to adjust the aircraft center of gravity and improve stability [2]. In the case of the configuration of HYPER, Sweep is needed to allow for a higher vertical distance and to allow for a reasonable range for the center of gravity.

The Dihedral angle of a wing has a high influence on the lateral stability of an aircraft. Its determination requires an in depth analysis of the aircrafts stability [2] that can not be provided at the current design stage. For a higher clearance angle between the ground and the propulsion system, a Dihedral of 9° is set.

To estimate the weight and structural characteristics of the wing, the airfoil thickness is needed. This parameter is of importance for a box wing concept, since the weight of the wing can be reduced when using an airfoil with a higher thickness to chord ratio (t/c ratio). Additionally, a higher t/c ratio improves the structural integrity of the

wing. Nevertheless, due to the box wing configuration, the absolute wing thickness is comparatively small, which brings aerodynamic benefits. According to an equation 7 suggested in [18], the maximum t/c ratio for this concept is 12%. The technology paramter k_M is assumed to be 0,932 and the Lift Coefficient for minimum drag is calculated with equation 8. According to these parameters, the weight of the wing can be estimated as outlined in Section 6.4.

$$\frac{t}{c} = 0.127 \cdot M^{-0.204} \cdot \cos\varphi^{0.573} \cdot C_{L,md}^{0.065} \cdot k_M^{0.556} \tag{7}$$

$$C_{L,md} = \sqrt{C_{D,0} \cdot \pi \cdot AR \cdot e_0} \tag{8}$$

Since the boxwing concept consists of two wings, there are different possibilities for the placement of control surfaces and high-lift devices. For this concept, the ailerons are placed on the trailing edges of both the upper and lower wings to control roll. In the configuration of HYPER, the rear wing fulfills the role of horizontal tail and the elevators are placed on its trailing edge. To increase the lift during takeoff and landing, Flaps are installed along the trailing and Slats on the leading edge of both wings [22].

4.3. Tail Geometry

The empennage is designed as a V-tail, with the stabilizers also acting as struts for the aft wing to enhance its stability as described in Section 4.1. The stabilizers have a Dihedral angle of 45°. As mentioned in Section 4.2, the aft wing serves as horizontal stabilizer. Consequently, the V-tail surfaces primarily function as vertical stabilizers. The exact size and geometry of the vertical stabilizer is dependent on requirements regarding stability and controllability. For a rough sizing during the preliminary design process, the vertical tail volume consisting of the product of the area and lever arm of the vertical tail, is used to determine the size of the empennage. Since the surfaces of the V-tail are angular, the projected area is used. It can be calculated using the chord length at the tip and root of the wing as well as the overall height of the tail.

$$S_V = 0.5 \cdot (cl_{r_V} + cl_{t_V}) \cdot h_V \tag{9}$$

For a smooth junction, the chord length at the tip of the V-tail is chosen to be the same as the chord of the aft wing. The height of the tail is determined by the height to span ratio and the diameter of the fuselage. The additional geometry parameters are chosen in accordance with [18] and can be found in table 23.

4.4. Lift and Drag

To investigate the drag behaviour of HYPER, the quadratic form of the drag polar is used.

$$C_D = C_{D,0} + \frac{C_L^2}{\pi A R e_0} \tag{10}$$

As can be seen in Formula 10 the drag is reduced with a higher span efficiency and Aspect Ratio as mentioned in Section 4.1 and 4.2. To determine the zero-lift drag coefficient $C_{D,0}$, the tool OpenVSP is utilized. OpenVSP is a parametric aircraft geometry tool that enables users to generate a 3D model of an aircraft using common engineering parameters. Following the creation of the model, OpenVSP's implementation of the panel method was employed to simulate aerodynamic behavior. This approach is applicable for subsonic speeds and provides adequate results for preliminary design phases. With this method, a coefficient of 0,021 is calculated which is consistent with comparable boxwing concepts [18].
To model the lift behaviour of the aircraft, the empirical formula 11 suggested by D. Scholz and D.Schiktanz [18] is applied to determine the lift curve slope shown in figure 5.

$$\frac{dC_L}{d\alpha} = \frac{2\pi AR}{2 + \sqrt{AR^2(1 + \tan^2\varphi - M^2) + 4}} \tag{11}$$

Using the slope, the lift coefficient for different angles of attack is calculated using formula 12. For this formula, the zero-lift angle of the airfoil α_0 is needed. Since biplanes are in need of airfoils with markedly different camber from those of monoplanes to prevent premature separation [23], no specific airfoil is chosen at this point. However, for the calculation of the lift coefficient, an angle of -2° is assumed since it is a typical value for airfoils used in aircraft of this size [2].

$$C_L = \frac{dC_L}{d\alpha}(\alpha - \alpha_0) \tag{12}$$

Based on these values, the lift-to-drag polar can be determined and is shown in Figure 7. The maximum Lift to Drag ratio is determined to be 20.7 using formula 13. This value aligns roughly with the typical maximum L/D ratios of boxwing aircrafts [18].

$$L/D_{\text{max}} = \frac{1}{2}\sqrt{\frac{\pi \cdot AR \cdot e_0}{C_{D,0}}} \tag{13}$$

4.5. Stability and controllability

When designing a bowing aircraft, longitudinal stability is one of the mayor challenges. This is particularly due to the conflict between stability and aerodynamic efficiency that occurs in such configurations. Two key conditions are essential for achieving stability and controllability. The stability condition, that requires the slope of the pitching moment about the center of gravity to be positive and the trim condition, that states that the pitching moment about the center of gravity has to be

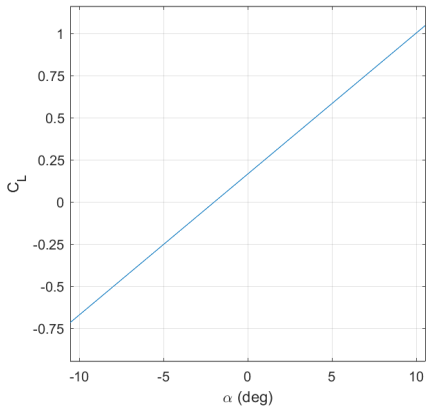

FIG 5. Lift Coefficient over Angle of Attack

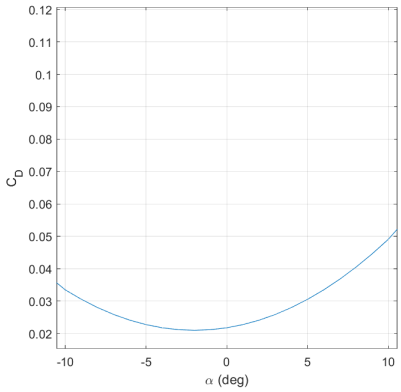

FIG 6. Drag Coefficient over Angle of Attack

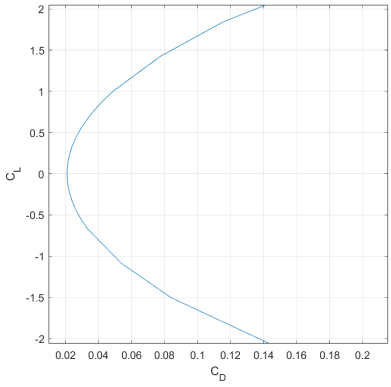

FIG 7. Lift-to-Drag Polar

positive at zero lift. Since both wings of a boxwing generate positive lift, it is difficult to provide a positive zero lift pitching moment to fulfill the trim requirement. To be able to do so, the front Wing has to provide more lift than the aft wing ($C_{L,1} > C_{L,2}$). However according to biplane theory a condition for minimum induced drag is that both wings generate an equal amount of lift. This circumstance limits the range of the center of gravity, as the trim condition is one of its constraints. An additional method to comply with both requirements is optimizing the horizontal distance between the fore and aft wings, as a greater distance enhances stability by reducing aerodynamic interference and improving control authority. Furthermore, adjusting the twist and sweep of the wings tailors the aerodynamic characteristics for stability. Wing twist helps control lift distribution along the span, reducing the risk of tip stall, while sweep affects the aerodynamic center's position and stability characteristics [18]. Balancing stability and aerodynamic efficiency requires trade-offs, as stability often necessitates deviations from optimal aerodynamic configurations. Achieving a practical design involves integrating aerodynamic, structural, and control considerations. At this stage of the design process, the stability of the concept cannot yet be reliably proven because factors such as the exact center of gravity of the aircraft depend on a detailed design and analysis. However, the feasibility of a stable concept for an aircraft of comparable size was shown in multiple studies such as [24] and [25].

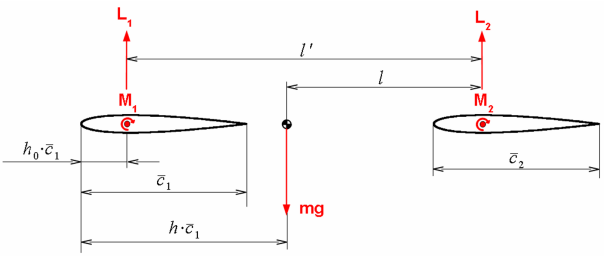

FIG 8. Forces and moments acting on a boxwing aircraft [26]

5. POWERTRAIN

When designing a fully electric aircraft, the powertrain, including the propulsion and power system, is of great importance for the overall energy efficiency of the concept since it has a direct influence on the aircraft's weight, energy consumption, and performance. Proper dimensioning ensures that each component operates within its optimal efficiency range, reducing energy losses and enhancing the sustainability and cost-effectiveness of the aircraft.

Advantages of such a concept include the elimination of hydraulics, which are typically heavy and require maintenance due to their complexity and susceptibility to contamination. Additionally, fully electric systems offer high efficiency and a uniform supply of power, resulting in a streamlined energy management system that reduces overall system complexity. This uniformity simplifies the integration of various power-dependent systems, promoting a more efficient and reliable aircraft design.

However, transitioning from combustion-based systems to an all-electric layout presents new challenges. For instance, the absence of bleed air, which is traditionally used for cabin climate control, necessitates the addition of alternative air inlets and compressors. Furthermore,

the protection against overload conditions and general system failures must be meticulously addressed in the system architecture. An example of such an approach to system protection and reliability is discussed in detail in Chapter 5.2.
The propulsion system of HYPER comprises two electric-driven propellers located under the wings and one boundary layer ingesting (BLI) fan at the rear. This configuration is meticulously selected to optimize the aircraft's performance, structural efficiency, and safety.

For thrust generation various possible rotor types were identified. One of them is the common propeller. Propellers are essential for both military and civilian aircraft due to their high propulsion efficiency and excellent take-off and landing performance. They are widely used in transport aircraft, UAVs, and electric aircraft. Recent advancements in propeller technology have mainly focused on reducing excessive noise. Noise reduction is crucial for meeting civil noise standards, as Europe aims for a 65% reduction in noise levels by 2050 compared to 2000, and enhancing cabin comfort. Unlike turbofans, propeller noise reduction must address the sound source directly through blade design, necessitating a multidisciplinary optimization approach to balance aerodynamic performance, strength, and noise reduction [27]. One of the projects focused on propeller noise reduction is the IRON project, part of Europe's Clean Sky 2 initiative within the regional aircraft package. The project aims to design innovative propeller concepts that significantly reduce noise levels without compromising aerodynamic performance [28].

Another possible concept is the ducted fan or shrouded propeller. A ducted fan, a propeller within a circular duct, is a hybrid between a propeller and a turbofan engine, where the duct acts like an annular wing. This concept has a lower noise level and less vibration. It provides better static performance than an open propeller at the same power, thanks to the suction effect at the duct inlet and higher static pressure at the outlet. However, ducted fans have drawbacks such as increased weight and drag from the shroud, poor performance at high duct angles of attack, and potential issues with inflow distortion and stalling on the inner duct side, especially during high-rate descents or under significant downwash flow. Aerodynamic forces and moments on the duct can also pose challenges [29].

While an electrically driven propeller is comparable to a turboprop engine, the ducted fan is more akin to a turbofan engine. The conventional propeller is better suited for lower speeds up to Mach 0.6 and is commonly used in smaller regional aircraft, whereas the ducted fan is more efficient at higher speeds. [30]. There are also open rotor designs that aim to combine the advantages of both concepts. While these designs could be even more aerodynamically efficient, they are less promising in terms of noise levels [31].

For a better comparison, the concepts were evaluated based on specific criteria (1-poor; 5-excellent). As shown, the conventional propeller received the highest rating and is therefore chosen for the wing-mounted engines, serving as the primary thrust generator. For the engine in the back, a ducted fan was choosen, as it is more efficient for boundary layer ingestion and spatially fits better due to the tail and fuselage.

TAB 2. Comparison of different thrust generation options

	Propeller	Ducted fan	Open rotor
Efficiency	4	4	5
Weight	4	1	2
Noise	3	4	1
Coasts	4	2	2
Complexity	4	2	2
	19	13	12

Opting for two propellers and one ducted fan, rather than additional engines, effectively reduces the complexity and weight of the electrical cabling required for power distribution. By limiting the number of engines, the design minimizes cabling, nacelle weight, and maintenance requirements, thus enhancing fuel efficiency and performance [2].
Only having two propellers in the front also enables a placement of the propellers near to the fuselage which offers significant structural benefits. In Boxwing aircraft, which have relatively thin wings, this arrangement reduces bending moments and stress on the wing structure, allowing for a lighter and more durable wing design.
From a safety perspective, having three engines provides essential redundancy. Should one engine fail, the remaining engines ensure continued safe operation, thus meeting safety standards [14] and enhancing flight stability.
To properly dimension the propulsion system, the most power demanding section of the flight mission must be considered, thus the take-off. At peak power 7952.104 kW in total is needed for the electric motors to provide the demanded thrust defined by the determined power loading (Chapter 4).
A propeller efficiency of 85% is assumed and already included. The efficiencies of the electric motors and the inverters are assumed to be 98% and 99% [32]. To generate thrust, the power supply therefore theoretically must deliver 8196.36. kW. As HYPER is a fully electric aircraft, no extra generator or APU is needed to provide electricity for the on board electronics. To meet the additional demands, the batteries or Fuel Cells must provide 3% more power. With this constant extra power of 238.6 kW, the onboard electrical systems can be adequately supplied [33].

5.0.1. Boundary Layer Ingestion

A method to reduce the drag, improve the efficiency and therefore decrease the propulsive power consumption of an aircraft is Bbundary layer ingestion (BLI). This reduces energy consumption per kilometre per passenger,

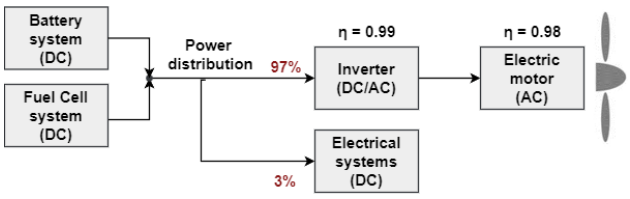

FIG 9. Propulsion system overview

environmental impact and direct operating costs. The concept of BLI is to minimize the required propulsion power by using an inflow with the lowest velocity possible for thrust generation [34]. Instead of ingesting the free stream flow and accelerate it to a higher velocity, the slower moving boundary layer flow is ingested and accelerated up to free stream velocity or higher [35].
The ideal BLI configuration would be to ingest one hundred percent of the boundary layer by the propulsor and assume that the wake is perfectly filled. However this ideal configuration would not be possible nor beneficial nor safe. Therefore an actual BLI configuration requires supplemental propulsion for example propellers under the wings [35].

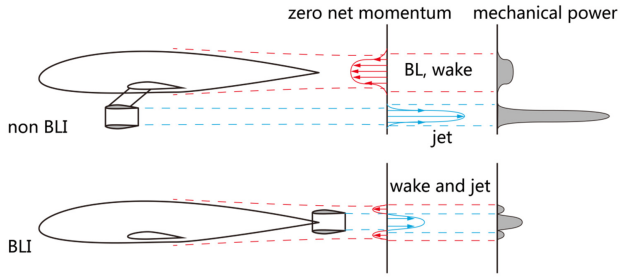

FIG 10. Drag reduction of BLI configuration

HYPER uses a full annular BLI located at the rear of the aeroplane as an electric fan. The BLI supplies 12% of the cruise power which corresponds to 5.4% at peak power. The generated thrust of the BLI is 2822.7 N. For a conventional engine like the two propellers under the wings, this would equal 451.63 kW. But as a BLI is more efficient and needs less power to provide the thrust, only 253.56 kW motor power is needed Therefore, it is only necessary to generate 7998.28 kW from the original 8196.36 kW to provide the maximum thrust [35].

5.0.2. Engines and Inverter

The configuration mentioned above is quantified as follows: 253.56 kW for the BLI fans' motor and 2838.12 kW for each of the wing-mounted motors. To estimate the power density of electric motors in 2050, a comprehensive market analysis was conducted. Particularly noteworthy were the electric motors from eMoSys GmbH, a subsidiary of MTU aero engines. These motors currently achieve a power density of 15 kW/kg, the highest available on the market today. At present, a typical powertrain operates at 600 kW, but higher outputs are expected by 2050. It is plausible that power levels in the single-digit megawatt range will become achievable. [36] Assuming this specific power density, the total weight of all the motors amounts to 540.96 kg. The weight is distributed proportional to the power: 16.9 kg for the BLI fans' motor and 255.87 kg for each of the wing-mounted motors.
Since the Power System of HYPER based on hydrogen fuel cells and batteries produces a direct current and electric motors operate using an alternating current, inverters are needed to connect these elements [6]. For the inverters a gravimetric power density of 30 kW/kg is assumed for EIS 2050 [37]. Accordingly the total weight of all inverters of HYPER is 264.33 kg.
The power density of electric motors and inverters is strongly dependant of the cooling system [6]. For this reason HYPER has a cryogenic cooling system using the liquid hydrogen as a coolant with a helium recirculation loop as it is done in the Airbus Cryoprop project [38]. For cryogenic cooling on airplanes a current TRL of 6 is estimated as there has been a demonstrator designed by Airbus but no actual flight qualified system [39] [40]. For the whole cooling system a weight of 305 kg has been assumed [41].

5.1. Power System

As described in the energy source selection, the power System for HYPER is entirely electric leading to a reduced complexity in the power system architecture. Hydrogen Fuel Cells and Batteries are used in a direct-hybrid configuration levering both their specific properties. During cruise, the aircraft utilizes the Fuel Cell system exclusively to take full advantage of hydrogen's high specific energy, thereby extending the range of the all-electric aircraft. For take-off and climb, when higher power is required, the battery, known for its high specific power, provides the additional power needed. This strategy ensures that the Fuel Cell system is not oversized, maintaining a lighter and more efficient system by optimizing the distinct advantages of both the Fuel Cell and the battery. Additionally, this strategy allows the range to be easily adapted solely by variing the fuel load [42].
As previously mentioned, the Fuel Cells are the sole providers of power during the cruise segment and thus are being dimensioned according to this phases demand. The difference in power during take-off and climb is compensated by the batteries. In addition to the power requirements of the propulsion system, the power for the additional onboard electricakl systems mentioned in chapter **??**

5.1.1. Hydrogen Fuel Cells

In general, Proton Exchange Membrane Fuel Cells (PEMFCs) and Solid Oxide Fuel Cells (SOFCs) are extensively researched for aviation applications, whereas PEMFCs are more common. This preference is attributed to several advantageous properties of PEMFCs such as their high power-to-weight ratio, leading to a lighter power system. They also achieve high energy conversion efficiency with a degree of efficiency of 60 %, optimizing fuel use and extending the operational range of the aircraft. In terms of durability, PEMFCs demonstrate reliability over long operational periods, meeting the rigorous demands of aviation applications. Another

significant advantage of PEMFCs is their rapid start-up capability and efficient load-following behavior. These characteristics are essential for meeting the varying power demands during different phases of flight, such as takeoff, cruising, and landing [43]. Depending on the type of proton conducting membrane, the operating temperature can vary, leading to the distinction between Low Temperature and High Temperature PEMFCs. For this concept, HT-PEMFCs are chosen. Their main advantages consist of their resilience towards impurities and the more efficient operation in comparison to LT-PEMFCs. Additionally, the larger temperature gradient facilitates the cooling process and therefor allows for a lighter cooling system, reducing the overall weight of the system [44].

5.1.2. Balance of Plant

For the proper operation of a Fuel Cell, several additional components, collectively known as the "Balance of Plant" (BoP), are required. These components consume power supplied by the Fuel Cell, thereby impacting its overall power output. Moreover, they add to the weight of the fuel system, necessitating an analysis of both their weight and power requirements. Two critical components of the Balance of Plant are the hydrogen and air supply systems. Hydrogen is delivered to the Fuel Cell via a connection that includes pipes and valves to control fuel flow from the hydrogen tank. Since liquid hydrogen is used as a fuel, the pipes need to be insulated to avoid boil-off leading to an augmented weight of the fuel transport system [45]. For air supply, which is drawn from the surrounding atmosphere, multiple preparatory steps are necessary before entering the Fuel Cell. The air must be filtered, compressed, cooled, and humidified to meet the fuel cell's requirements [44]. Another vital component of the Balance of Plant is the thermal management of the Fuel Cells, as approximately 50 percent of the hydrogen's specific energy is converted into heat. To maintain the Fuel Cell's efficiency, the operating temperature must be maintained. Given the substantial power requirements and the connected heat production, a liquid cooling system is used in this application. The main advantages of such a cooling system consist of its high heat transfer coefficients and the ability to maintain uniform temperature distribution across the Fuel Cell stack. Additionally, the efficiency of the Fuel Cell system can be augmented by recovering the waste heat. By including heat exchangers in the system, the waste heat can be utilized for usecases such as environmental control of the cabin and de-icing of the wings [46]. Furthermore, the voltage output from the Fuel Cell stacks must be adjusted for various components in the aircraft. This adjustment is achieved using a DC/DC converter. Finally, all BoP components require coordination by a central electric control system to ensure proper operation and integration. The layout of the the Fuel Cell system is depicted in Figure 11.

To approximate the weight of the fuel cell system in HYPER, a rough sizing of the fuel cell and its Balance of Plant is done according to the methodology suggested by M. C. Massaro et al. [47]. In general, the Fuel Cell System is dimensioned according to its required maximum power output. As a gravimetric power density, 5 kW/kg is chosen for the Fuel Cell stacks and 3 kW/kg for the entire system in accordance with current prognostics for the development of HT-PEMFCs until the EIS [48] [49]. The resulting weight of the Fuel Cell System is depicted in Table 3.

5.1.3. Hydrogen Tank

Another importent component of the fuel system is the hydrogen storage system. Due to hydrogen's inherently low density at ambient temperature and the resulting reduced energy density per unit volume, a large storage volume is needed. This presents several challenges in a industry such as aviation, where compact designs, minimal weight and safety are essential. Two key parameters for the evaluation and comparison of different technologies are the Gravimetric Density (n_g in %) and the Volumetric Density (n_v in MJ/l). The Gravimetric Density is defined as the weight of the contained hydrogen in relation to the total mass of the storage system. The Volumetric Density is given by the ratio between the energy content of the stored hydrogen and the total system volume [47].

In general, the methods for the storage of hydrogen can be divided into two categories. Those being material based and physical based technologies. For the first method, hydrogen is stored through the adsorption into other Materials by chemical bonds or physical forces. Examples for sorbents or hydrides are metal organic frameworks, metal hydrides or chemicals such as Ammonia [50]. Because of the low technology readiness levels, the complexity in handling and the augmented system weight [47], these storage solutions are not investgated further for this application. On the other hand, physical based storage methods store hydrogen in its molecular form either compressed, liquified or cryo-compressed. When comparing the characteristics of these storage methods, liquid hydrogen storage emerges as the most suitable method for the given task. Liquid hydrogen storage offers superior energy densities, both gravimetric and volumetric, compared to compressed hydrogen, leading to a lighter and more compact system [47]. Additionally, storing hydrogen as a liquid requires maintaining near-ambient pressure (about 1.5 bar), significantly enhancing safety by mitigating the risks associated with high-pressure storage systems used in compressed hydrogen [51]. Liquid hydrogen technology is relatively mature and commercially available, with a technology readiness level (TRL) of 9. Furthermore, ongoing advancements in tank materials and insulation technologies are expected to further reduce system weight and enhance safety. The refueling process for liquid hydrogen is both fast and reliable, a crucial factor for maintaining operational efficiency in aviation [52]. The primary challenge of liquid hydrogen storage is the

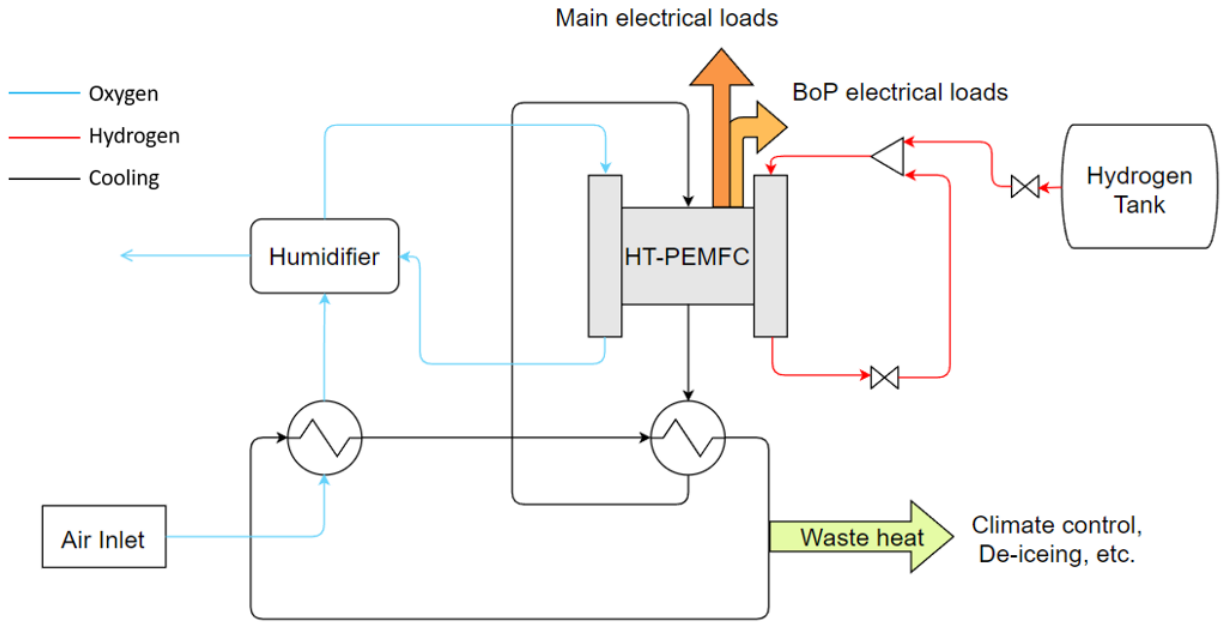

FIG 11. Schematic structure of the Fuel Cell System

boil-off phenomenon, where hydrogen evaporates due to heat transfer, increasing tank pressure. To mitigate this, tanks should be equipped with multilayer insulation to reduce thermal conductivity, and designs that favor spherical shapes and larger sizes to minimize the surface area-to-volume ratio [47].

To make the best use of the advantages and disadvantages of liquid hydrogen, the hydrogen tank for HYPER is designed to be spherical to achieve minimal boil-off. To approximate the size of the tank, the volumetric density of storage concepts for liquid hydrogen is used that lies at 6.4 MJ/l [52]. According to current research, a Gravimetric density of up to 75 % can be achieved for larger tanks when using advanced composite materials such as carbon fiber reinforced polymers and reducing the thermal load and therefor the need for heavy structural components by using improved material for the insulation [53]. For a more conservative approach, a Gravimetric density of 60 % is assumed for the weight calculation to account for this future development.

5.1.4. Fuel calculation

For the dimensioning of the tank and the calculation of the maximum take-off weight, the fuel mass for the longest range has to be determined. In the case of HYPER the mission with the largest range is the connection between HAM and SSJ with a distance of 1250 km. This decision is based on the specific characteristics of hydrogen and its storage. As the maximum range of the aircraft extends, the hydrogen tank becomes larger both in volume and weight leading to a larger fuselage and augmented MTOW. These parameters reduce energy efficiency for shorter missions considerably. Therefore, an analysis of the required energy for different maximum ranges is conducted with the optimal range being 1250 km optimizing both energy efficiency and operating cost by reducing the need for stopovers during longer missions. This is presented in depth in section 7.2.

For the calculation of the fuel weight, equation 14 is used [47].

$$M_{H_2} = \frac{1}{\mathrm{LHV}_{H_2}} \int_0^{t_{\mathrm{end}}} \frac{P_{\mathrm{el,\ mission}}(t)}{\eta_{\mathrm{FC}}}\, dt \tag{14}$$

To apply this equation, the energy provided through the conversion of hydrogen is determined by calculating the electrical power output of the Fuel Cells in each flight phase as well as the duration of the segments. With a Lower Heating Value (LHV) of 119.96 MJ/kg and a Fuel Cell efficiency η_{FC} of 60%, the fuel mass is calculated. In addition to take-off, climb, cruise, descent and landing, the fuel for a go-around, a flight to an alternate airport (250 km diversion range) and 30 minutes holding are taken into account. In addition to that, 5% contingency fuel is added as well as another 5 % to account for boil-off effects of the liquid hydrogen. For the design mission the total fuel amounts to 659.4 kg with 441.7 kg being used for the mission at hand. The weight of the fuel and tank system are presented in Table 3.

5.1.5. Batteries

In addition to hydrogen fuel cells, the aircraft is equipped with advanced batteries that provide supplementary power. These batteries are essential for supporting peak power demands during critical phases of flight, such as take-off and climb. They also serve as a backup power source, ensuring reliability and safety.
For the usage in aviation, batteries need to adhere to certain standards regarding safety, efficiency, weight etc. As estimated by the Head of DLR Institute of Electrified

Aircraft Propulsion the energy density of batteries increases by 5 % every year [5]. For EIS 2050 assuming the technology level of 2045 to account for certification and testing, this means an energy density of almost 700 Wh/kg will be available for HYPER. According to the "Alternative Battery Technologies – Roadmap 2030+"by Fraunhofer this assumption is realistic for new, innovative Battery technologies [7]. The most suitable and common current technology used for electric flight projects is Lithium-Ion Batteries. However, Lithium-ion batteries (LIBs) present challenges in aviation, especially for larger and regional aircraft, due to their relatively low energy density. Promising alternative technologies are anticipated to become viable by 2050, including metal-ion, metal-sulfur, and metal-air batteries, as well as redox flow batteries. The most promising technologies for aviation are Lithium-sulfur (Li-S) and Lithium-air (Li-air) batteries.
Li-S batteries could achieve higher gravimetric energy density than LIBs but face challenges with volumetric energy density and cycle stability. Due to the high energy density and the low cost of sulfur, Li-S batteries also have the potential to achieve a low cost per kWh. Improvements in cycle stability and power density are required and expected until 2050. An energy density of 550 Wh/kg is expected until 2035.
Lithium-air (Li-air) batteries, despite their low technology readiness level (TRL), offer extremely high gravimetric energy density of up to 1230 Wh/kg and potentially lower costs than LIBs, contingent upon solving their cycle stability issues. [7]
Considering the range of advanced battery technologies, lithium-air batteries emerge as the most promising option for HYPER. Despite their current low TRL, the potential for a high gravimetric energy density, combined with potentially lower costs than LIBs, makes them an attractive choice. The primary challenge is the cycle stability, but ongoing research and development are expected to address this issue, making Li-air batteries a viable and efficient energy solution for an EIS 2050 aircraft.
As mentioned above, for the presented aircraft an energy density of 700 Wh/kg is assumed on system level. This value already includes the Battery management system and module cooling.
As the fuel cells are designed to have a maximum power output of 3496 kW (as in cruise) and the peak power that needs to be provided is 7998.28 kW, 4502.28 kW need to be provided by the batteries. Considering the flight envelope and formula 15, this corresponds to an energy of 521.9 kWh.

$$E_{\text{Bat,min}} = \sum_{i=\text{Take off}}^{\text{Climb}} E_{\text{propulsion},i} - \sum_{i=\text{Take off}}^{\text{Climb}} E_{\text{FC},i} \tag{15}$$

In order to achieve the required energy and voltage level the single battery cells are connected in series. The nominal voltage of a Li-air cell is approximately 3 V [54].
The nominal operating voltage level of the battery system is 800 V which is based on the Airbus EcoPulse High Voltage Battery [55]. In the battery system 24 V modules are used consisting of 8 cells with a capacity of 100 Ah at 3 V. In order to build the 800 V battery system 34 of these modules are needed. The energy content of one module is 2.4 kWh.
The energy provided by all modules connected in series is 81.6 kWh
Moreover, it must be noted that only 80% of a battery capacity can be used in order increase the lifespan of the battery [6]. Therefore, the usable energy of one string is 65.28 kWh.
After that, the number of parallel strings is calculated as the following:

$$n_{\text{strings}} = \frac{E_{\text{Bat, goal}}}{E_{80}} = 8$$

Computing the mass of the battery pack is similar to the calculation for fuel cells. The differences are the input variables like energy of the battery pack and its gravimetric energy density. In total, the battery system is assumed to weight 932.57 kg. With a volumetric energy density of 600 Wh/l [32] the volume is 1.187 m3.
To reduce turnaround times, the Fuel Cells can run continuously. This is necessary for HT PEMFC's due to their start-up times and can also extend their overall lifespan. During taxi-in and taxi-out operations active charging of the batteries is performed in order to not waste the excess power. Additionally, if the FCs are slightly oversized, the batteries could be recharged during cruise as shown in Figure 12, minimizing or eliminating the need for charging at the gate. This active charging during the mission introduces a slight increase in the aircraft's weight due to the additional fuel and slightly higher power output during cruise, which amounts to an additional 27.8 kg of hydrogen. Nevertheless, this weight increase is minimal and does not significantly affect the aircraft's overall performance. An alternative to reduce turnaround times is the battery exchange method at the airport, but this approach would necessitate additional time, infrastructure, and personnel, as well as substantial modifications to the aircraft's architecture. Compared to the relatively small weight increase from charging the battery during flight, the constant replacement of batteries would be more costly and involve greater risks due to the potential for battery damage.

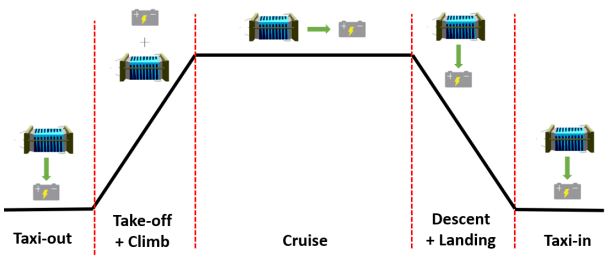

FIG 12. Power management Fuel Cell and Battery

5.2. Powertrain Architecture and Overview

To ensure proper operation of the aircraft, all the individual components of the powertrain have to be

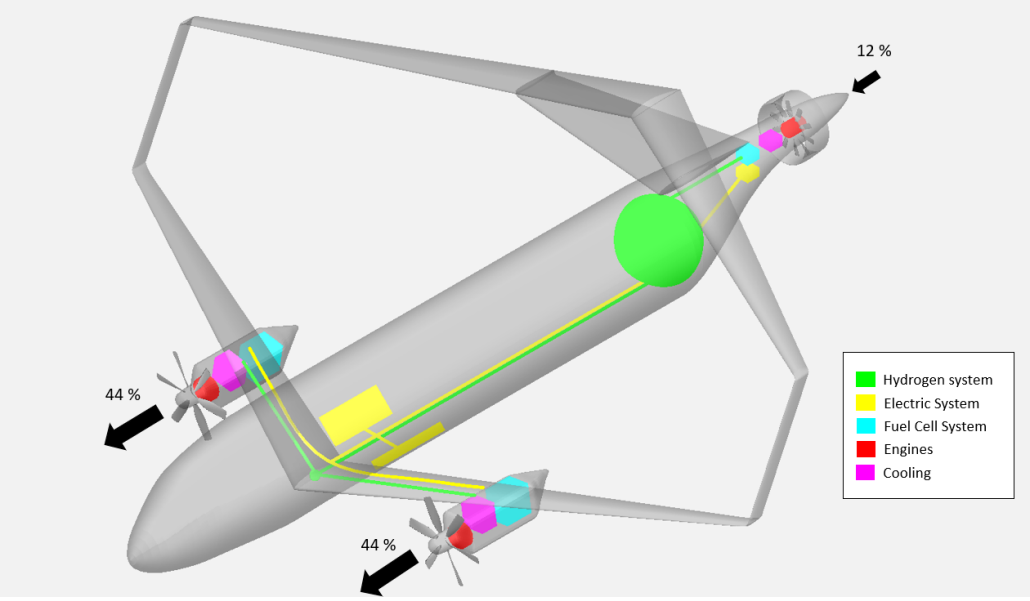

FIG 13. Position of Power Train Components

strategically interconnected and placed inside of the aircraft. In order to reduce the length of cabeling and therefore ohmic losses, each propulsion system is fueled by an individual power system consisting of a battery pack and fuel cell stacks that are placed near the motors. This layout additionally ensures the independence of each propulsion system from the others. However, should a failure of a component in one of the propulsion systems occur, it is advantageous if the remaining functional components can be used to support the rest of the system [56]. For that reason, the fuel cells are connected to the batteries within each individual power system. Additionally, the batteries are connected to enable exchange of electricity. That way, in case of the failure of a motor, the hydrogen fuel cell can continue producing electricity, that can be used for charging the battery. To provide protection from hazardous overvoltage and other malfunctioning, circuit protective devices such as circuit breakers are installed to deenergise and disconnect faulty power sources and power transmission equipment from their associated busses. This layout ensures conformance of the powertrain architecture with CS-25 requirements [56]. To enable the proper operation of the entire system, a central control unit is needed. This unit monitors the state of charge of the batteries, the hydrogen levels in the tank, and the performance of the fuel cells. It dynamically adjusts the power output from the fuel cells and batteries to match the power demand of the aircraft's propulsion system and other onboard systems.

The position of the individual components is depicted in figure 13. The weight of the individual components is depicted in table 3 and their current technology readiness levels in table 4. It is assumed that technologies with a current TLR higher than or equal to 3 will reach Level 8 or 9 until the EIS.

TAB 3. Mass Estimation Powertrain

Component	Mass in kg
FC Stack	621.2
BoP	414.1
Battery	1110.9
Tank	610.6
Pipes	100
Electric motors	541.5
Inverter	270.8
Propeller	414.6
BLI fan	100
Nacelles	409.9

TAB 4. TRL Powertrain Components

Component	Current TRL
HT-PEMFC	6 [57]
Liquid Hydrogen storage	8-9 [58]
BLI	3-4 [59]
Cryogenic cooling	6 [40]
Li-air batteries	3 [7]

6. AIRCRAFT CONFIGURATION

In addition to the wings and powertrain, other components of the aircraft configuration are crucial for meeting design requirements and achieving design objectives. To develop a comprehensive concept, the optimization goals are considered in each component and throughout every stage of the design process.

6.1. Structure and Material

In the development of the aircraft, selecting the ideal materials for the individual components plays a central role. The materials used in an aircraft should ideally be well-suited for their specific application and durable, while also being lightweight. Load-bearing structures of the aircraft are critical and must be made from sufficiently safe materials. Aluminum alloys and carbon fiber composites have been selected for these materials. However, the secondary structures in the aircraft do not need to be as strong. For example, in the cabin of the aircraft, ceiling panels or overhead bins can be replaced with components made from natural fibers, which are more resource-efficient and lighter. The goal is to predominantly use pure, sustainably produced biomaterials in aircraft construction by the year 2050 (Ref. [60], [2]).

6.2. Cabin and Fuselage

For conventional aircraft, the primary functions of the fuselage are to house the payload and passengers. Typically, fuel is stored in the wings, and the sources for thrust, such as jet engines, are also commonly located on or near the wings. However for HYPER, such a configuration is impractical. The main sources of energy, the fuel cells and batteries, cannot be fully accommodated within the wings due to geometric constraints. Furthermore, as discussed in section 5.1.3, the hydrogen tank needs to be cylindrical to minimize boil off. In combination with its high volume, this tank configuration therefore cannot be housed within the wings either. Thus the fuselage must be designed to not only serve its conventional purposes of accomodating passengers and cargo but also of efficiently incorporating the hydrogen tank and batteries.

FIG 14. Sideview fuselage

Preferably the tank is located behind the passenger cabin as seen in figure 14. Alternatively the tank can also be placed between the passenger cabin and cockpit to change the center of gravity. Disadvantageously, this constellation would then mean that the flight attendants can no longer enter the cockpit. For example in case of an emergency in the cockpit flight attendants can no longer support midflight. Another drawback is that if the fuel cells are located in the back of the aircraft hydrogen pipes are significantly longer, therefore heavier and less efficient.

Given these unique constraints, the design of the fuselage must prioritize the efficient integration of fuel cells and hydrogen tanks while maintaining structural integrity and minimizing drag. Achieving low aerodynamic drag is essential for optimizing the aircraft's performance. To determine the optimal low-drag-configuration the fineness ratio is used. This ratio relates the length of the fuselage to its maximum diameter. For low drag configuration it has a value of approximately six which results in a short but wide aircraft. For longer, thinner configurations this ratio can go up to 14 which leads to higher drag but also leads to smaller sized vertical and horizontal stabilizers (Roskam). For the first iteration of the design phase a fineness ratio of eight should be aimed for as this can be adjusted if required so.

The next step involves the dimensioning of the cross section starting with the passenger cabin. This is crucial as it, in combination with the fineness ratio, the passenger number and the needed volumes for batteries and hydrogen, allows for the derivation of all dimensions relevant for the fuselage sizing. The passenger cabin itself consists of the seat rows, aisles, galley and the lavatory as seen in Figure 15.

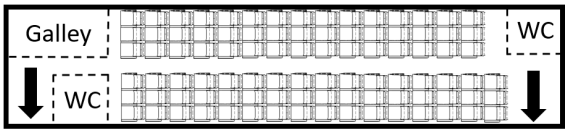

FIG 15. Example cabin layout

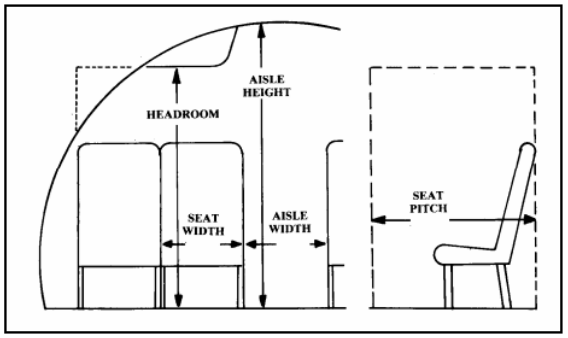

FIG 16. Seat dimensions [61]

Placement of the exits can be varied if blocked by the wing structure as the minimum distance from each seat to the exit is always lower then the required 18.3 m [14]. To determine length, width and height of the cabin, the named features as seen in figure 16 are defined as following:

TAB 5. Common cabin and seat dimensions [61]

	Economy	High density
Seat pitch (in.)	34 - 36	30 - 32
Seat width (in.)	17 - 22	16 - 18
Headroom (in.)	> 65	-
Aisle width (in.)	18 - 20	≥ 12
Aisle height (in.)	> 76	> 60
Passengers per staff	31 - 36	≤ 50
Passengers per lavatory	40 - 60	40 - 60
Galley volume per passenger ($ft^3/pass$)	1 - 2	0 - 1

TAB 6. Cabin and seat dimensions for HYPER

	Dimensions (in.)
Seat pitch	32
Seat width	16
Headroom	65
Aisle width	$2 \cdot 15$
Aisle height	76

The values in table 6 primarily base on commonly used cabin and seat dimension for high-density aircrafts [table 5] as space management is critical for this concepts fuselage design [61].

Regarding the aisle configuration two significant designs decisions are implemented. The aisle width is increased to 15 in as for certification this is the minimum width in this aircraft size category [14]. Additionally the concept opts for a twin aisle layout, even though such configuration is unconventional for this aircraft size. However, this design decision reduces boarding time by up to 50% and therefore improves passenger experience significantly [62]. This is additionally improved by implementing foldable seating concepts for the seats adjacent to the aisles. When storing the carry-on baggage in the overhead compartments, passengers can fold up the seat bottoms, move out of the way and therefore do not block the aisles.

This results in a layout of 15 rows, with six passenger seats. As the optimal determined passenger number is 89 and this configuration having 90 PAX, one seat remains, which is intended for a flight attendant. Regarding the number of crew members this concept needs two to three flight attendants, one pilot and one co-pilot. It also needs two lavatories and a galley volume of approximately 90 f^3. These values also base on common characteristics for high-density aircrafts [61]. This leads to a cabin length of

$$f_{\text{cabin}} = n_{\text{rows}} * l_{\text{seat}} + l_{\text{galley}} + l_{\text{wc}} \tag{16}$$
$$f_{\text{cabin}} = 13.45m$$

Note: The lengths of lavatory and galley are both defined as 1.01 m to simplify calculations.

and the cross section as seen in figure 17.

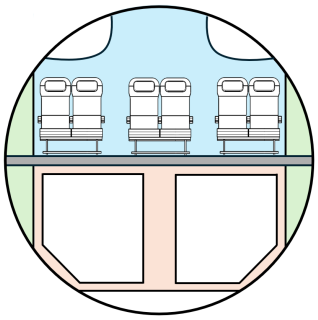

FIG 17. Crossection fuselage

In comparison to conventional aircraft designs this concepts passenger cabin ends with a vertical wall at the outboard seats. This creates an empty space between the cabin and the fuselages outer wall (green), which can be utilized as the batteries storage while providing windows. This fusion of batteries and wall is common along latest eVTOL-technology [63], which means certification should be no potential risk as these designs expect certification in the upcoming years.

Beneath the passenger cabin is the cargo compartment, used or storing the passengers luggage Therefore this section is primarily dimensioned through the estimated luggage per passenger. This configuration results in a fuselage diameter of 3.68 m. It is maximum at the cabin / cargo section and consistent along the fuselage as this makes manufacturing more efficient and cheaper. Additionally it simplifies the implementation of a pressure cabin.

To fully determine the dimensions of the fuselage the lengths of rear, nose and tank are missing. As described in section 5.1.3 the hydrogen tank is spherical.

$$V_{\text{tank}} = \frac{1}{6} \cdot \pi \cdot d_{\text{tank}}^3 \tag{17}$$

$$l_{\text{tank}} = l_{\text{fuse}} = 3.68\text{m} \tag{18}$$

To determine lengths of nose and rear sections it is assumed these lengths are proportional to the diameter, which results in the following equations:

$$l_{\text{nose}} = 1.5 \cdot d_{\text{fuse}} = 5.52\text{m} \tag{19}$$

$$l_{\text{rear}} = 2 \cdot d_{\text{fuse}} = 7.36\text{m} \tag{20}$$

Note: Nose and tail are not modelled properly at this stage. The dependency between length of nose or rear to the maximum fuselage diameter is an estimation to simplify calculations. To properly determine optimal dimensions further calculations and simulations have to be done.

This results in the following fuselage length:

$$l_{\text{fuse}} = l_{\text{nose}} + l_{\text{tank}} + l_{\text{cabin}} + l_{\text{rear}} \tag{21}$$
$$l_{\text{fuse}} = 29.31\text{m}$$

6.3. Landing Gear

This section outlines the parameterization and design process for the landing gear. The procedure is carried out in accordance with the method described in [2]. Key parameters influencing the parameterization of the landing gear are the height of the landing gear and the center of gravity.
The height of the landing gear is determined by specified guidelines for the aircraft's ground clearance, measured from the lowest point of the aircraft to the ground. The Propellor Clearance was set to 0.5 m, according to CS 25.925 [14]. The height of the Landing Gear is calculated with $x \approx 1.8m$ as the vertical distance between the middle of the propellor and the gravity center: [2]

$$H_{cg} = \Delta H_{clear} + \frac{D_{prop}}{2} + x \approx 3.8\,\text{m} \tag{22}$$

A weight distribution was chosen with a load of 15% on the nose wheel. Based on empirical data and comparisons, a wheelbase of 12.4 meters is selected. From these data, the distance of the main landing gear to the center of gravity can be determined as follows: [2]

$$\frac{F_{nose}}{MTOW}! = 15\% \leftrightarrow F_{nose} = 0.15 \cdot MTOW \tag{23}$$

$$b = \frac{F_{nose} \cdot 12.4m}{MTOW \cdot g} = 1.86\,\text{m} \tag{24}$$

Furthermore the weight can be calculated from empirical values and the wingspan b, as well as the height of the landing gear as follows: [2]

(25)

$$W_{LG} = K_L \cdot K_{ret} \cdot K_{LG} \cdot W_L \cdot \left(\frac{H_{LG}}{b}\right) \cdot \eta_{\text{ult}_{land}}^{0.2}$$

Additionaly, the minimum track width is calculated as follows: [2]

$$TW > 2\frac{F_C \cdot H_{cg}}{mg} \text{ with } F_C = MTOW \cdot \frac{V_{taxi}^2}{R_r} \tag{26}$$

$$F_C = 89896.35\,\text{N} \tag{27}$$

$$TW_{min} = 2.44\,\text{m} \tag{28}$$

It is to say, that Input parameter of the minimum track width are for example the Taxi-Speed, which was set to $35^{km}/_{h}$. This is the maximum speed the aircraft may theoretically experience while performing a turning radius maneuver of 30 meters. It should be noted, however, that for safety reasons, such tight turning maneuvers are usually performed at lower speeds. [64] [65]
Based on the collected data, the requirements that the landing gear must meet can be established. Using these data, the weight of the landing gear can be calculated with high accuracy according to Formula 25. Due to the distribution of the center of gravity explained in Chapter 6.5, a tricycle configuration was selected as the concept, in which the main landing gear, with the adjusted track width, absorbs approximately 85% of the primary loads. To ensure compliance with the track width and propeller clearance while maintaining retractability of the landing gear, a track width of 2.6 meters was chosen. Ultimately, all characteristic values from the chapter can be compiled (Table 7).
In order to attach the landing gear to the aircraft, but without wings in the center of the aircraft as mounting points due to the chosen configuration, appropriate boxes must be designed. Unfortunately, these boxes have a negative impact on the aerodynamics of the aircraft aerodynamics. However, this effect remains within manageable limits and does not lead to a fundamental deterioration of the aircraft's aerodynamics. Additionally, the landing gear does not retract laterally.
Furthermore, after comparisons with similar-sized aircraft, tires with a width of 0.27 m and a diameter of 0.86 m for the main gear and a width of 0.165 m and a diameter of 0.559 m for the nose gear were selected. [2] [66] The collected data regarding the landing gear design can be found in Table 7.

TAB 7. Landing Gear Data

Parameter	Value [m]
LG Vertical Height	3.8
Wheel Base	12.4
Main Gear to c_g	1.86
Min. Track width	2.44
Tire Diameter Main	0.86
Tire Width Main	0.27
Tire Diameter Nose	0.56
Tire Width Nose	0.17
Configuration	Tricycle

6.4. Mass Budget

To design the components, an initial mass estimation is necessary. This was carried out according to the methods described in [2]. The initial mass estimation resulted in an estimated total mass for the maximum takeoff weight of approximately $MTOW \approx 35000kg$. In the mass calculation phase, the components are now calculated, allowing for the mass to be determined more precisely. This step is performed iteratively until negligible changes occur. The mass is continuously recalculated using the methods presented in this chapter.
After all components have been designed, the mass of the aircraft can be calculated with an accuracy of 80% to 95% [2]. This is done according to the steps described in [2] and [18].

In general, the weight consists of empty weight, payload, crew, and fuel. Since the payload and crew weight change minimally compared to the initial estimate, only the empty weight and fuel weight require calculation. While the calculation of the fuel weight has already been explained in 5.1.4, this chapter will describe the calculation of the empty weight. This includes various structural weights such as the fuselage, wings, and V-Tail, as well as weights of the landing gear. Since insufficient empirical values are available for the weight calculation of the wings for a boxwing configuration, the wing weight must be calculated using Formula 29. A description of the procedure for calculating the wing weight can be found in 6.4.1.

6.4.1. Calculation of the Wing Weight

$$m_W = S_W \cdot MAC \cdot \left(\frac{t}{C}\right)_{max} \cdot \rho_{mat} \cdot K_\rho \cdot \left(\frac{AR \cdot \eta_{ult}}{cos(\Lambda_{0.25})}\right) \cdot \lambda^{0.04} \quad (29)$$

The formula used for the mass calculation of the wing 29 is derived from [2]. The parameters are obtained from material data and wing geometry. The empirical value K_ρ, which describes the so-called "Wing Density Factor", is derived from tables in [2]. It is a parameter that describes the stability of the wing; for example, it takes a higher value when the engines are mounted on the wing compared to when they are mounted on the fuselage. To validate the results of the calculated wing weight a comparison with the wings calculated in [18] has been done. This yields a wing weight of approximately $m_W \approx 6111.09$kg for the wing combination, with the weight distribution as derived from [18].

- $m_{W,forward} \approx 3499.51$kg
- $m_{W,aft} \approx 2611.58$kg

The collected data can be utilized to create a weight table (Tab. 8), listing all significant weight values. It should also be noted that the weight of the systems and equipment varies for the designed aircraft. For example, the de-icing of the wings is achieved using waste heat from the fuel cells, eliminating the need for a dedicated de-icing system. It should be noted that the "engine weight" includes the weights of the FC stack, electrical motors, inverter, nacelle, BLI, and propeller, while the "engine systems weight" encompasses the weights of the balance of plant and cooling systems. The "fuel system weight" includes the weight of the pipes. The individual weight data of the Propulsion System can be found in Tab 3.

6.5. Center of Gravity

Since the placement of the center of gravity (CG) is critical for ensuring stability and controllability of a boxwing aircraft, it has to be investigated to ensure general feasibility of the design. Since the front wing generates more lift than the rear wing (as required for stability), the CG should be between the wings, but closer to the front wing to ensure a stable pitching moment. This placement helps maintain a positive static margin, which is the distance between the center of gravity and the neutral point (NP), providing a buffer for stability [26]. With this objective and using the weight of the individual components presented in the previous chapter, the center of gravity is roughly calculated for different layouts of the aircraft's interior and wing positioning. According to this analysis, the layout discussed in Section 5.2 and 6.2 can be feasible. The exact center of gravity is dependant on the detailed structural design and loading and can therefore not be exactly determined at the present time.

TAB 8. Weight distribution of HYPER

Parameter	Mass (kg)
Fuel	659.41
Landing Gear	1,426.6
Engines	2,276.3
Engine Systems	726.92
Fuel Systems	100
Systems and Equipment	1,569.2
Wings	6,110.9
Tail	772.2
Fuselage	4,642.7
Battery	1,110.86
Tank	395.64
Payload	8,455
Crew	285.76
MTOW	28,532
MZFW	27,872
OEW	19,131

7. EVALUATION OF THE OPTIMIZATION TARGETS

To evaluate the performance of HYPER in regard to its two primary optimization targets during the design process, the energy consumption and Direct Operating Costs (DOC) are analysed in detail. Additionally, a comparative assessment is conducted against the Dash 8 Q400, an established benchmark in regional aviation.

7.1. Reference aircraft

The De Havilland DHV-8-400, commonly known as the Dash 8Q-400 (hereafter referred to as "Dash 8"), is a twin-engine turboprop aircraft developed and manufactured by the Canadian aerospace company De Havilland Aircraft of Canada, formerly known as De Havilland Canada, during the 1980s. Building on the success and popularity of the Dash 8 series, the Dash 8-400 was introduced with notable upgrades, such as advanced engines and enhanced aerodynamics. Capable of seating up to 90 passengers, the Dash 8-400 currently stands as

the highest capacity turboprop in the market, offering the lowest unit cost. The aircraft is optimized for regional networks, capable of operating within a range of up to 2000 km.
Beyond its passenger configurations, the Dash 8-400 is highly versatile and adept at performing various utility missions. It achieves 40% greater range and 30% higher cruise speeds compared to typical turboprops, establishing it as the most efficient turboprop currently available [67].

Given its dominant market position and low production costs, the Dash 8-400 was selected as the reference aircraft for calculations and estimations during the preliminary design phase. It aligns well with the mission envelope defined by this year's challenge, which includes operating within a maximum range of 1482 km and matching our determined range requirements. Additionally, the Dash 8-400's passenger capacity and preliminary Maximum Takeoff Weight (MTOW) align with our estimations 6.4.
The specifications of Dash 8-400 in latest standard configuration, according to the manufacturer's data sheet, are listed in Table 9.

TAB 9. DHC-8-400 Specifications

Parameter	DHC-8-400
PAX	82
MTOW [kg]	30,481
MLW [kg]	29,030
OEW [kg]	17,903
Fuel [kg]	5,138
Range [km]	2037
Maximum Cruise Speed [km/h]	667
TO Field Length [m]	1163-1277
Landing Field Length [m]	1268
Maximum Cruise Altitude [m]	7620

7.2. Energy consumption

Since HYPER uses the advantages in drag reduction and high Lift/Drag-ratio of a boxwing configuration and a BLI fan as well as a highly efficient and lightweight powertrain, the aircraft flies in a very efficient manner. For the determination of the energy consumption in each mission segment, the consumed energy provided by the Fuel Cells and the Batteries is determined. According to these values, the performance parameter Energy/PAX/km is calculated. When calculating the fuel mass and size of the batteries according to the consumed energy in each mission section, flight phases such as go around, diversion and holding where taken into account. However, for this calculation, an ideal mission progression is assumed. The energy requirements in each flight phase of the main design mission HAM-SJJ are listed in table 10.
The required energy varies in each mission according to the range and the MTOW. To give an overview of the general energy consumption of HYPER, the

TAB 10. Energy consumption during the flight envelope for HAM-SJJ

Mission Segment	Consumed Energy in MJ
Taxiing (in and out)	3531.6
Take-off	380.3
Climb	2586.5
Cruise	19662.4
Descend	308.8
Approach and Landing	29.5
Total	26499.1

Energy/PAX/km of the shortest and longest missions are depicted in table 11 that can be completed without stopover. Additionally, the longest mission using a stopover is showcased. For all of them, maximum Passenger capacity is assumed as well as an ideal mission progression.

TAB 11. Energy/PAX/km for different missions

Route	Energy/PAX/km in kJ/PAX/km
GOT-VBY	389.5
HAM-SJJ	238.2
BRI-SZG-HAM	280.4

To be able to assess these values in relation to the current market, the energy consumption of the reference aircraft Dash 8 is estimated and used as a means of comparison. This performance indicator is estimated according to the aircrafts fuel consumption. Depending on the mission, the fuel consumption can vary between 0.0147 and 0.0221 kg/PAX/mi according to a study conducted by Aircraft commerce [68]. The variation is rooted in factors such as the traveled distance, the maximum take-off weight and the weather conditions during the analysis. Using the lower heating value of 43,1 MJ/kg of kerosene [69] the estimated energy consumption amounts to a range of 387.9 to 603.4 kJ/PAX/km.

When compared across different routes, the energy per passenger per kilometer (Energy/PAX/km) for HYPER is significantly lower, with values ranging from 238.2 kJ/PAX/km to 389.5 kJ/PAX/km. This efficient energy performance underscores the potential of HYPER to reduce operational costs and environmental impact, positioning it favorably against conventional aircraft such as the Dash 8.

7.3. Economic Analysis and DOC

The chosen concept relies partially on hydrogen, which is converted into electrical energy within fuel cells, and on electrical energy directly obtained from batteries. Hence, for the calculation of direct operating costs (DOC) the model proposed by Hoelzen et al. [70], based on Thorbeck's DOC assessment method [71] applies. The

hybrid propulsion concept is analogously adjusted for the DOC calculation as indicated in the task description.

The DOC are calculated according to Hoelzen as follows ([70], Formula 1):

$$DOC_{total,yearly} = DOC_{cap} + DOC_{maint} + DOC_{crew} + DOC_{fees,ATC} + DOC_{fees,airport} + DOC_{energy} \tag{30}$$

As evident from the formulas, the DOC of HYPER is divided into various components, each calculated individually. The respective calculations are comprehensively explained in Hoelzen et al. [70] or its referenced sources. Consequently, not all formulas are detailed or repeated in this paper. Instead, this section focuses on the details and assumptions made for developing the DOC of HYPER. The values used in the formulas are presented in tabular form in this paper, categorized by the respective DOC section they pertain to. Values directly adopted from sources are marked accordingly (Ref.).

Note: Since Hoelzen et al. do not differentiate between the values provided by Thorbeck, despite them being in $€_{2013}$, no such distinction is made here either. Values are presented in absolute terms without conversion factors for currency nor year, ensuring direct comparability. Given that the source [70] frequently references $\$_{2020}$ and the task specifies energy prices in $\$_{2019}$, DOCs here are also simplified and presented in $\$_{2020}$, since the difference between these years is considered negligible.

Respective weights are not detailed in the following DOC calculations; instead, the reader is referred to Tab. 3 and 8 for this information.

7.3.1. Yearly Flight Cycles and Flight Time

While capital and crew costs are independent of the yearly operational flight time ($OT_{p.a.}$) — since capital costs account for general aircraft price, based on factors like mortgage and depreciation periods, and insurance and maintenance - various air traffic control airport-related fees, and energy costs need to be scaled with yearly flight cycles (YFCs) and flight time (FT).

Thorbeck [71] provides a standard formula for determining these figures based on potential yearly operation time ($POT_{p.a.}$), average stage length (R_{av}), cruise speed (v), block time (BT), and yearly forced downtime ($DT_{p.a.}$):

$$YFC = \frac{OT_{p.a.}}{\frac{R_{avg}}{v} + BT} \tag{31}$$

The general input data is shown in Table 12. R_{av} is calculated as the mean average of all airport-to-airport (including stopovers) flights within the given network.

TAB 12. YFC Input Data

Parameter	Value
$OT_{p.a.}$	6011.2 h (Ref. [71])
BT	2.3 h (Ref. [70])
R_{avg}	717.375 km
v	576 km/h

This yields a total of **1696 YFCs**. FT is the ratio of v to R_{avg} and results in **0.8 h**.

7.3.2. Capital Costs

According to Hoelzen et al. [70] (Formula A7), the capital costs comprise the price per aircraft (P_{AC}) multiplied by the annuity factor (a) and the insurance rate (f_{ins}). This approach is similar to Thorbeck's, with the exception that the price per aircraft is not linearly related to the MTOW but rather depends on a comprehensive set of factors, including the additional weight of alternative energy sources and related systems. The annuity factor is calculated based on input data from the reference, as shown in Table 13.

TAB 13. Annuity Factor

Parameter	Value
IR	5 %
f_{ins}	0.5 %
f_{RV}	0.05
DP	14 years
a	0.0984

The price per aircraft consists of recurring costs (RCs), non-recurring costs (NRCs), a profit margin (PM_{AC}), and a miscellaneous factor (f_{misc}). RCs account for individual components and systems, engines, load and handling costs, final assembly and delivery, and engine costs. While Hoelzen does not provide a calculation method, he references the approach by Beltramo et al. [72] for kerosene-driven aircraft, which is applied in Risse's "CeRAS" [73] and adopted for this paper. The respective costs are listed in Table 14 below:

TAB 14. Recurring Costs for Kerosene Aircraft

Recurring cost of system	Value [$]
C_i	21,292,002.40
$C_{LoadAndHandling}$	0
$C_{FinalAssemblyAndDelivery}$	5,323,000.61
C_{eng}	4,049,052.47
$RC_{Kerosene}$	30,664,055.47

Respective weights for calculations are considered according to Table 8. However, here engine weight includes fuel cells, inverter, electric motors and propeller for all engines and nacelles are respected individually. Since no further load or handling equipment as defined by

Beltramo [72] is required for ground handling of the aircraft, respective costs amount to 0.

Considering propulsion concepts using alternative energy sources, Hoelzen adds the product of stored energy (E_i) and a respective cost factor (k_i). This generalized approach is utilized in this paper as follows:

$$RC = RC_{kerosene} + \sum_i E_i \cdot k_i \tag{32}$$

HYPER's hybrid propulsion concept of batteries and hydrogen results in the input depicted in Table 15.

TAB 15. Recurring Costs for HYPER

Parameter	Value
$E_{stored,max,LH2}$	659.5 kg
$k_{stored,max,LH2}$	650 \$/kg$_{LH2}$ (Ref. [70])
$E_{stored,max,BAT}$	609.7 kWh
$k_{stored,max,BAT}$	200 \$/kg$_{LH2}$
RC	31,214,670.50 \$

The EU Clean Aviation initiative published a "Strategic Research and Innovation Agenda" in 2021 [74], which estimates development costs for each new aircraft type at €15 billion. This figure is adopted for NRCs, acknowledging that HYPER's key technologies involve significant research and development efforts. RCs are finally added with NRCs over an determined aircraft number (4000 acc. to [70]) and multiplied with factors for the PM_{AC} and a f_{misc} for e.g. spare parts. The PM_{AC} of 20% is directly adopted from Hoelzen [70] and for for the factor 2% are assumed. **The final capital direct operating costs amount to 4,413,827.43 \$**.

7.3.3. Maintenance Costs

For alternative energy sources or hybrid concepts, Hoelzen does not estimate any changes in maintenance costs. They are adapted from Thorbeck's DOC model and divided into: Airframe Material Maintenance Costs, Airframe Personnel Maintenance Costs and Engine Maintenance Costs (see Table 16).

TAB 16. Maintenance costs

Parameter	Value
FT	0.8 h
$DOC_{Maint,AF,Material}$	547,503.51 \$
LR	50 \$/h (Ref. [71])
B	2 (Ref. [71])
$DOC_{Maint,AF,Pers}$	286,158.14 \$
n_{eng}	3
$T_{SL,Static}$	5.1 t
$DOC_{Maint,Engine}$	217,787.05 \$

The total yearly maintenance costs consequently amount to 1,050,885.98 \$.

7.4. Crew Costs

Like maintenance cost, Hoelzen refers to crew costs calculation outlined by Thorbeck [71], through linear scaling of crew complements required for the operation of a single aircraft, using the average annual salaries of cockpit crew (S_{FC}) and flight attendants (S_{FA}). The number of flight attendants is determined by either scaling by payload handled (one for each 5000 kg) or maximum passenger numbers (one for each 50 PAX), with the latter approach being used here, since it is certification standard [71]. The following input parameters are applied, as referenced by Thorbeck [71]:

TAB 17. Crew costs

Parameter	Value
CC	5 (Ref. [71])
S_{FA}	60000 \$ (Ref. [71])
S_{FC}	300000 \$ (Ref. [71])

Crew costs result in 2,100,000.00 \$ per year.

7.4.1. Airport Fees

The airport fees are linearly scaled with payload and take-off weight for handling and landing fees as follows ([70], Formulas A1 and A2):

TAB 18. Airport fees

Parameter	Value [kg/\$]
$P_{handling}$	0.1 (Ref. [70])
$P_{landing}$	0.01 (Ref. [70])

Resulting from the inputs and weights in Table 8. the landing costs amount to 1,319,250.60 \$, and the handling costs are 445,190.50 \$.

7.4.2. Air Traffic Control Fees

The air traffic control (ATC) fees are calculated by multiplying an ATC cost factor (f_{ATC}) with range and the square root of MTOW divided by 50 as presented by Hoelzen (Formula A3, [70]). Input is as follows:

TAB 19. Air traffic control fees

Parameter	Value
f_{ATC}	0.5 (Ref. [70])
R	1250 km

Annual ATC fees amount to 432,360.64 \$ considering the MTOW from Table 8.

7.4.3. Energy Costs

To determine the energy costs, Formula A2 from [70] was utilized. The energy costs assumed for the EIS year 2050 were provided in this year's assignment, as shown in Table 20. Block energy (BE) consumption is based on Table 10, but converted into kWh. Since the aircraft recharges

its batteries during cruise, there are no additional energy costs for recharging at the airport, resulting in zero costs for this aspect.

TAB 20. Energy

Parameter	Value
P_{LH2}	0.097 $/kWh
$BE_{LH2,mission}$	7360.9 kWh
$BE_{LH2,p.a.}$	12,484,086.4 kWh
P_{Bat}	0.038 $/kWh
$BE_{Bat,Mission}$	0 kWh
$BE_{Bat,p.a.}$	0 kWh

Total DOC of energy results in 1,210,956.38 $.

7.4.4. DOC for HYPER

Table 21 presents the detailed DOC components for the HYPER aircraft, along with the aggregate value. A comprehensive evaluation and comparison with the reference aircraft, the Dash 8, are illustrated in Figure 18 in Chapter 7.4.6.

TAB 21. HYPER DOC

Parameter	Value [$]
DOC_{cap}	4,413,827.43
DOC_{maint}	1,051,448.70
DOC_{crew}	2,100,000.00
$DOC_{fees,ATC}$	432,360.64
$DOC_{fees,Airport}$	1,764,441.06
DOC_{energy}	1,210,956.38
DOC_{HYPER}	10,973,034.21

By utilizing the computed DOC values and the annual flight cycles, it is possible to determine the minimum ticket price required for the HYPER aircraft to achieve profitability. The break-even ticket price per passenger per flight is 72.70 $.

7.4.5. DOC for DHC-8-Q400

The DOC for the Dash 8 Q400 is calculated using the model developed by Thorbeck [71] for kerosene-powered aircraft, as outlined in the task statement.

Detailed calculations of the individual values are omitted here. Instead, a summary of the DOC values for the Dash 8 Q400 is provided. These calculations are performed under the same operational conditions as those for the HYPER aircraft to facilitate direct comparison. Given the Dash 8's range, R_{avg} is set at 765.07 km, and no stopovers are required. Based on the performance data of the DHC-8-400 provided in Section7.1 and a reduced BT of 1.83 hours related to conventional kerosene-based propulsion (Ref. [71], [70]), YFCs amount to 2020 and FT to 0.9 h.

Table 22 displays the DOC components for the Dash 8 Q400, analogous to the analysis provided for the HYPER aircraft.

TAB 22. DOC Dash 8 Q400

Parameter	Value [$]
DOC_{cap}	2,323,113.74
DOC_{maint}	1,169,145.06
DOC_{crew}	2,100,000.00
$DOC_{fees,ATC}$	3,212,713.53
$DOC_{fees,Airport}$	2,588,448.20
DOC_{fuel}	1,492,278.80
DOC_{D8}	12,868,790.67

The break-even ticket price per passenger per flight is 71.60 $.

7.4.6. DOC Evaluation

The HYPER aircraft and the Dash 8 Q400 reveal significant differences in financial efficiency. A breakdown of individual DOC components of HYPER and DHC-8-400 is presented in Figure 18.

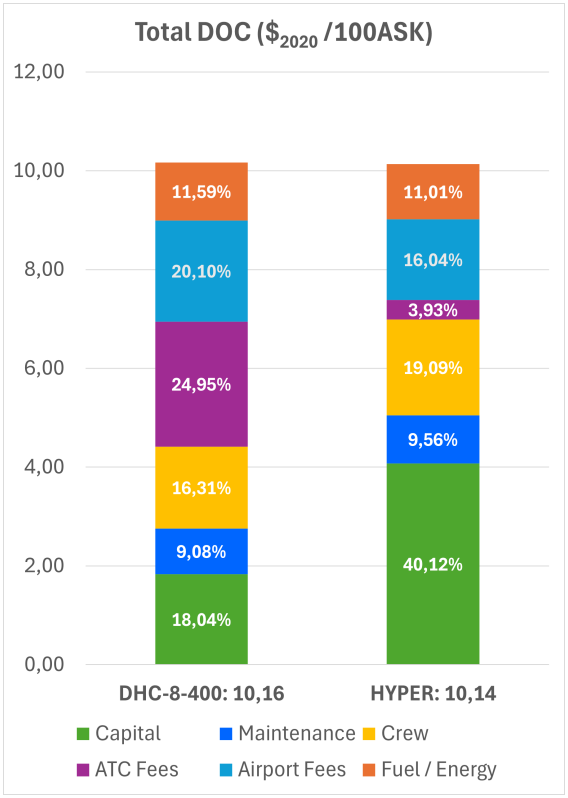

FIG 18. DOC evaluation of HYPER

First, the similarities between the two aircraft are examined, followed by an analysis of the differences and their origins.
Crew costs are unsurprisingly identical, as passenger capacity is within the same range and the number of flight attendants is proportional to every 50 passengers. Consequently, both DOC models allocate a similar share to crew costs.

Similarly, maintenance costs exhibit comparable values. This alignment is expected, given that Hoelzen's DOC model [70] does not incorporate the potentially higher maintenance costs associated with alternative propulsion systems. Hoelzen et al. [70] estimate an 11% increase in maintenance costs for hydrogen-powered aircraft, particularly for short-range operations. Despite this, applying the 11% increase would not surpass the maintenance costs of the Dash 8, demonstrating HYPER's competitive position in this regard. This efficiency is attributed to relatively short flight durations, low thrust per engine distributed across three engines, and the use of a boundary layer ingestion (BLI) fan during cruise.

Surprisingly, the fuel or energy costs are similar for both aircraft, despite kerosene being a more cost-efficient energy source. The boxwing configuration of HYPER plays a crucial role here, as it significantly reduces drag and enhances energy efficiency. Additionally, recharging batteries saves approximately 30,000$ annually, based on a battery energy demand of 436.6 kWh for the design mission. Furthermore, hydrogen as an energy source contributes to greater energy efficiency.

The most significant differences between the two aircraft's DOC are observed in capital costs, air traffic control (ATC) fees, and airport fees.

As detailed in Section 7.4.2, the calculation uses linear scaling of range. The Dash 8's higher range results in elevated ATC fees. Additionally, its specifications lead to higher airport fees compared to HYPER, due to differences in maximum takeoff weight (MTOW) and handled payload (see Section 7.4.1). Although ATC fees have a more substantial impact on the overall DOC, airport fees for both aircraft are within a similar value range.

The capital costs exhibit the most pronounced disparity, both in terms of overall share within the DOC and in absolute figures. This discrepancy is primarily due to the high non-recurring costs (NRC) of HYPER, driven by the substantial development expenses associated with the novel boxwing design and next-generation propulsion system.

Evaluating these factors, while the HYPER aircraft represents advancements in sustainability and energy efficiency, the operating costs of both aircraft remain within a comparable range.

Looking ahead, there is potential for further improvements in DOC, particularly with regard to crew costs. Typically, a cockpit crew comprises a pilot and a co-pilot. However, advancements in technology may enable the implementation of single-pilot operations (SiPO) concepts [75]. The feasibility of SiPO will hinge on technological progress, regulatory changes, safety assurances, and industry acceptance. The evolution of these factors over the coming years will be crucial in determining the viability of SiPO.

For this analysis, crew costs are based on the standard cockpit crew of two pilots, as the adaptation of SiPO by the Entry into Service (EIS) year 2050 remains uncertain. Nonetheless, adopting the SiPO concept could halve flight crew costs, reducing them to 1,350,000$ and thereby achieving a savings of 750,000$.

Looking ahead, there is potential for further improvements in DOC, particularly concerning crew costs. Typically, the cockpit crew consists of a pilot and a co-pilot. However, advancements in technology may facilitate the adoption of single-pilot operations (SiPO) concepts [75]. The feasibility of SiPO will depend on progress in technology, regulatory changes, safety assurances, and industry acceptance. The developments in the coming years will be pivotal in assessing the viability of SiPO. For these reasons, crew costs are calculated based on the standard cockpit crew of two pilots, since adaptation for the EIS year 2050 is questionable.However, implementing the SiPO concept could reduce flight crew costs by 50%, lowering them to 1,350,000 $ and resulting in a savings of 750,000 $.

8. DESIGN OVERVIEW

In the following sections, the final design specifications for the HYPER aircraft concept is presented. The provided tables offer a comprehensive overview of the aircraft's geometry and dimensions, performance metrics, and payload-range capabilities. Additionally, a detailed description of the operational concept for the HYPER aircraft at airports is included.

8.1. Aircraft dimensions

This section summarizes HYPER's dimensions in Table 23 and Figure 19.

TAB 23. Dimensions and geometry of HYPER

Parameter	Value
Fuselage	
Diameter	3.68 m
Length	30.16 m
Wing	
Wingspan	25.5 m
Area	67.7 m^2
Aspect ratio	9.6
Taper ratio	0.28
Dihedral (top)	0°
Dihedral (bottom)	9°
Sweep (top)	-25°
Sweep (bottom)	25°
Height to span ratio	0.2
Tail	
Unit area	22.2 m^2
Sweep	-30°

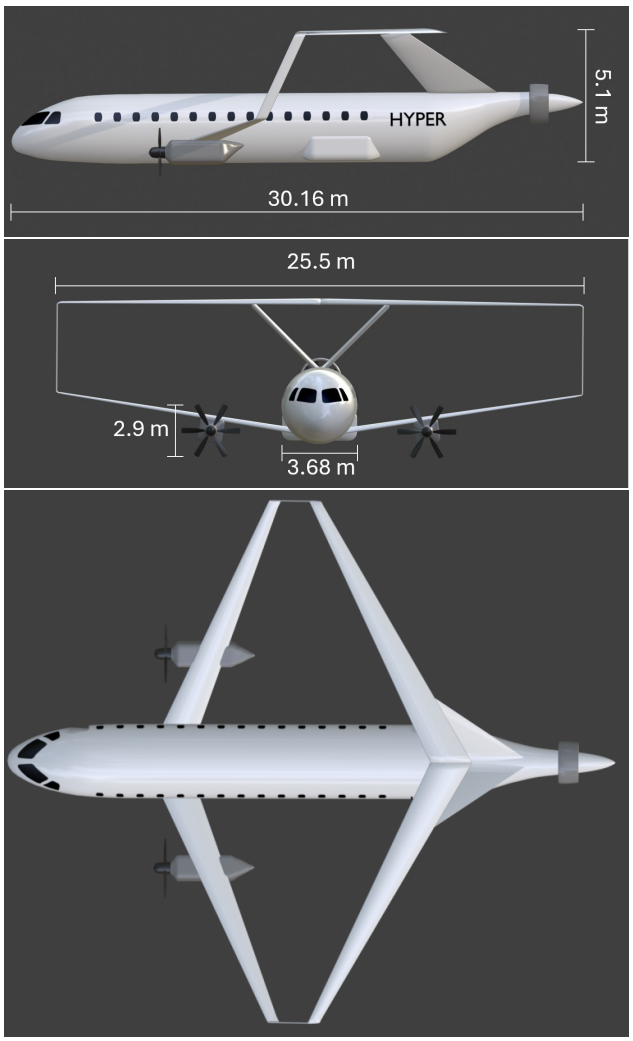

FIG 19. Three-sided view of HYPER

8.2. Aircraft performance

Tables 24 contains the key mission parameters of the concept. These include climb rate, cruising speed and altitude, aerodynamic and propulsion characteristics (e.g. glide ratio, energy consumption). Compared to the requirements as mentioned in Chapter 3.1 it can be said that all requirements are fulfilled.

TAB 24. Key mission parameters

Mission parameter	HYPER
PAX	89
Range	1250 km
MTOW	28,532 kg
OEM	19,131 kg
Payload	8,455 kg
Take-off field length	1223.5 m
Landing field length	1426.5 m
Climb rate	17 m/s
Cruise speed	160 m/s
Cruise altitude	8000 m
L/D (cruise)	19.7

8.3. Payload-range diagram

A payload-range diagram is a crucial tool for understanding the performance capabilities of an aircraft, particularly its trade-off between payload capacity and range. Compared to other aircrafts payload-range-diagrams, HYPERs is special. That is because usually the payload or weight decreases during operations as kerosene is burned to generate thrust. As the energy sources for the HYPER are hydrogen and batteries this is only partially true. The weight of the hydrogen decreases constantly, primarily during horizontal flight. But the weight of the batteries does not decrease with energy consumption. To be precisely the weight increases as the lithium-ions oxidizes. This increase is only marginal and therefore neglected for this payload-range diagram.

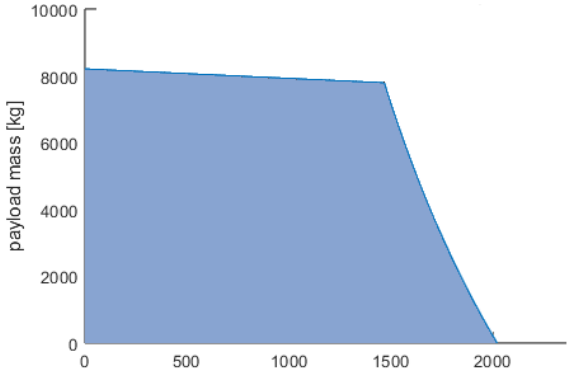

FIG 20. Payload-range diagram

8.4. Fueling and gate operations

When designing and developing an aircraft, ground handling and the compatibility of the design with airport structure have to be evaluated in order to ensure the concept to be holistic. As HYPER has a wingspan of 25.5 m it falls within the wingspan range of conventional aircrafts of this size. Therefore, airport access is not negatively influenced by the unconventional configuration and existing infrastructure for ground operations can be used. As HYPER's main engines are situated below the wings and the BLI engine can be found in the aft section, existing infrastructure can be utilized for maintenance. Additionally, even though handling fees for the DOC are estimated according to the weight of the payload and thus factors such as turnaround time are not considered in the absolute values representing the DOC, HYPER is designed to roughly match current conditions in order to keep this estimation realistic and ground operations as efficient as possible. Because of the twin isle concept of the cabin, boarding and deboarding of the passengers can be conducted in a time efficient manner. Additionally, since the cargo area is not disrupted by the wingbox, loading and unloading can be done simultaneously through dual cargo doors further augmenting efficiency.

The greatest difference between HYPER and conventional kerosene-based concepts lies in the refueling process. Nevertheless, refueling of LH2 tanks is comparable

to conventional ones with an approximated flow rate of about 900 l/min [76]. With a maximum fuel load of 659.4 kg, the refueling process can take up to ten minutes aligning with current standards for such a process in airport operations. On the other hand, the large timespans for loading numerous battery packs might pose a problem for efficient turnaround. For that reason, the power output of the hydrogen fuel cells is set to be slightly larger than the energy demand for the propulsion system and auxiliary electrical equipment of the aircraft during flight. The additional produced electricity is used to charge the on board batteries, making use of the entire cruise, descend and landing segment. This way, the aircraft arrives at the gate with fully charged batteries. An additional advantage of this concept consist of a higher level of redundancy during flight, as additional power arsenals are build up and can be used in case of component failure. Since the HT-PEMFCs used in this concept have a startup time of around 30 minutes, the Fuel Cells are continuously employed during gate operations, providing the required electricity in this phase.

9. DISCUSSION AND OUTLOOK

As previously outlined, HYPER includes numerous diverse and innovative concepts. This leads to several challenges, as these concepts are currently being tested and applied mostly in isolation. The combination of fully electric aircraft with propellers, box wings, and boundary layer ingestion necessitates several compromises. Nevertheless, when properly harmonizing the components in order to leverage their specific advantages, great qualities in relation to several future goals can be achieved. The box wing configuration offers significant aerodynamic advantages and propellers are the most efficient and lightweight means of generating thrust. Additionally, the optimized power system utilizing hydrogen as an alternative energy source ensures nearly emission-free flight and the BLI fan in the back reduces drag and fuel consumption. The wide fuselage of HYPER, provided by the box-wing configuration, allows for an almost ideal shape of the hydrogen tank, as mentioned in Chapter 5.1.3. HYPER aims not to focus on a single innovative concept but to integrate multiple ideas to yield optimal results. Despite the challenges, this approach is crucial to ensure that aviation has a sustainable future.

In conclusion, the development of a hybrid aircraft incorporating both battery and fuel cell technologies showcases a significant step forward in the pursuit of sustainable aviation. The rapid advancements in battery energy density and fuel cell efficiency are paving the way for extended range and increased payload capabilities, making hybrid aircraft increasingly viable for a broad range of applications. Furthermore, the potential integration of superconducting motors and inverters, despite their current low TRL, offers a promising future direction for achieving even greater efficiency and weight reduction in powertrains.

The synergy between advanced batteries and fuel cells not only enhances the operational flexibility of hybrid aircraft but also mitigates the limitations associated with each technology when used independently. As these technologies continue to evolve, the hybrid concept stands to benefit from continuous improvements, driving further reductions in carbon emissions and operational costs.

Contact address:

hennige.lena-it22@it.dhbw-ravensburg.de

References

[1] Europäische Kommission. european green deal. https://commission.europa.eu/strategy-and-policy/priorities-2019-2024/european-green-deal_de, 2024. Accessed: 14.07.2024.

[2] M.H. Sadraey, P. Belobaba, J. Cooper, R. Langton, and A. Seabridge. *Aircraft Design: A Systems Engineering Approach*. Aerospace Series. Wiley, 2012. ISBN: 9781118352809.

[3] Clean Sky 2 JU and FCH 2 JU. *Hydrogen-Powered Aviation*. Publications Office of the European Union, Luxembourg, May 2020. ISBN 978-92-9246-342-7 (PDF), doi:10.2843/471510.

[4] Ralf Peters. *Brennstoffzellensysteme in der Luftfahrt*. Springer Vieweg, 2015.

[5] Frank Lassak. *Fly Green - Nachhaltige Luftfahrt*. DLR, Motorbuchverlag, 2023.

[6] Dr.-Ing. Nejat Mahdavi. Electric and Hybrid Aircraft, 2023.

[7] Fraunhofer. Alternative Battery Technologies Roadmap 2030+, 2023.

[8] German Environment Agency. Kurzeinschätzung von Ammoniak als Energieträger und Transportmedium für Wasserstoff: Stärken, Schwächen, Chancen und Risiken, February 2022. Accessed: 16.07.2024.

[9] PhD Jayant Mukhopadhaya and PhD Brandon Graver. Performance analysis of regional electric aircraft, July 2022. White Paper, The International Council on Clean Transportation (ICCT).

[10] IATA. FACT SHEET 7: Liquid hydrogen as a potential lowcarbon fuel for aviation. https://www.iata.org/contentassets/d13875e9ed784f75bac90f000760e998/fact_sheet7-hydrogen-fact-sheet_072020.pdf, 2019. Accessed: 12.07.2024.

[11] Thomas Klaus, Carla Vollmer, Kathrin Werner, Harry Lehmann, and Klaus Müschen. Energieziel 2050: 100% strom aus erneuerbaren quellen, 2010.

[12] Deutsche Gesetzliche Unfallversicherung (DGUV). *Brandschutz beim Umgang mit Lithium-Ionen-Batterien*. Berlin, Germany, 1 edition, February 2024. DGUV Information 205-041.

[13] Deutscher Bundestag. *Verhalten von Elektroautos im Brandfall*. Berlin, Germany, wd 8 - 3000 - 002/22 edition, February 2022. Wissenschaftliche Dienste, Abschluss der Arbeit: 22. Februar 2022, Fachbereich: WD 8: Umwelt, Naturschutz und Reaktorsicherheit, Bildung und Forschung.

[14] EASA. Certification Specifications and Acceptable Means of Compliance for Large Aeroplanes (CS-25). https://www.easa.europa.eu/en/document-library/certification-specifications/group/cs-25-large-aeroplanes#cs-25-large-aeroplanes, 2023. Accessed 07.07.2024.

[15] Sergey V. Lyapunov Sergey L. Chernyshev and Andrey V. Wolkov. Modern problems of aircraft aerodynamics. *Advances in Aerodynamics*, 2019.

[16] Scholz Dieter Schicktanz Daniel. Das Boxwing Flugzeug. In *Ingenieurspiegel, Nr.2, S.20-25*, 2012. Download: http://Airport2030.ProfScholz.de.

[17] Meiko; Hecker Peter Schönhals, Shanna; Steen. Prediction, Detection and Avoidance of Wake Vortices Using Onboard Systems. In *CEAS: 3rd CEAS AirSpace Conference*, 2011.

[18] Daniel Schiktanz and Dieter Scholz. BOX WING FUNDAMENTALS – AN AIRCRAFT DESIGN PERSPECTIVE, 09 2011.

[19] Roy H. Lange, Jones F. Cahill, E. S. Bradley, R. R. Eudaily, C. M. Jenness, and D. G. Macwilkinson. Feasibility study of the transonic biplane concept for transport aircraft application, 1974.

[20] Dieter Scholz. Skript zur Vorlesung Flugzeugentwurf, 1999. Aircraft Design Lecture Notes.

[21] Egbert Torenbeek. *Synthesis of Subsonic Airplane Design*. Delft University Press, 1982. ISBN: 90-247-2724-3.

[22] Giuseppe Iezzi. PrandtlPlane High Lift System Preliminary Aerodynamic Design, 2006. Accessed: 2024-06-28.

[23] Paul Jemitola and Paul Okonkwo. An Analysis of Aerodynamic Design Issues of Box-Wing Aircraft. *Journal of Aviation Technology and Engineering*, 12, 09 2023. DOI: 10.7771/2159-6670.1253.

[24] Stephen Andrews and Ruben Perez. Stability and Control Effects on the Design Optimization of a Box-Wing Aircraft, 06 2014. DOI: 10.2514/6.2014-2592.

[25] Daniel Schiktanz. Conceptual Design of a Medium Range Box Wing Aircraft. https://www.fzt.haw-hamburg.de/pers/Scholz/arbeiten/TextSchiktanzMaster.pdf, 06 2011.

[26] D. Schiktanz and Dieter Scholz. The Conflict of Aerodynamic Efficiency and Static Longitudinal Stability of Box Wing Aircraft, 2011.

[27] D. Xue, Q. Yan, Z. Li, and K. Wei. Multidisciplinary optimization design of low-noise propellers. *Aerospace*, 10(10):254, 2023. Academic Editors: Hua-Dong Yao and Konstantinos Kontis. DOI: 10.3390/aerospace10030254.

[28] Centro Italiano Ricerche Aerospaziali (CIRA). The iron project, the future of regional aviation - researching innovative, low-noise propeller designs, 2024. Online article.

[29] T. Zhang and G. N. Barakos. Review on ducted fans for compound rotorcraft. *Aeronautical Journal*, 124(1277):941–974, 2020. DOI: 10.1017/aer.2019.164.

[30] Matthias Koppe. Kraftstoffverbräuche von turbofan, propfan und turboprop im vergleich, August 2012. Projekt.

[31] Dale E. Van Zante. Progress in open rotor research: A u.s. perspective. In *Proceedings of ASME Turbo Expo 2015: Turbine Technical Conference and Exposition*, Montréal, Canada, June 15–19 2015. ASME, American Society of Mechanical Engineers.

[32] m. Schmelcher and J. Häßy. Hydrogen fuel cells for aviation? A potential analysis comparing different thrust categories. *DLR*, 2022.

[33] A.J. Wileman, Sohaib Aslam, and Suresh Perinpanayagam. A road map for reliable power electronics for more electric aircraft. *Progress in Aerospace Sciences*, 127:100739, 2021. DOI: https://doi.org/10.1016/j.paerosci.2021.100739.

[34] Nils Budziszewski, Jens Friedrichs. Modelling of a Boundary Layer Ingestion Propulsor. https://www.mdpi.com/1996-1073/11/4/708, 2018. Accessed: 15.06.2024.

[35] Brennan T. Blumenthal, Alaa Elmiligui, Karl A. Geiselhart, Richard L. Campbell, Mark D. Maughmer, Sven Schmitz. Computational Investigation of a Boundary-Layer Ingesting Propulsion System for the Common Research Model. https://ntrs.nasa.gov/api/citations/20160010174/downloads/20160010174.pdf. Accessed: 15.06.2024.

[36] MTU Aero Engines. MTU Aero Engines entwickelt Technologie für fliegende Brennstoffzelle, 2023. Press Release.

[37] Christopher Hall, Chrysoula L. Pastra, Andrew Burrell, Jonathan Gladin, and Dimitri N. Mavris. Projecting Power Converter Specific Power Through 2050 for Aerospace Applications. In *2022 IEEE Transportation Electrification Conference Expo (ITEC)*, pages 760–765, 2022. DOI: 10.1109/ITEC53557.2022.9813991.

[38] Airbus Media. Airbus takes superconductivity research for hydrogen-powered aircraft a step further. https://bit.ly/4bSRPgZ, 2024. Accessed: 12.07.2024.

[39] Catherine G. Manning. Technology readiness levels. https://nasa.gov/directorates/somd/space-communications-navigation-program/technology-readiness-levels/, September 2023. Accessed: 2023-09-27.

[40] Airbus. Cryogenics and superconductivity for aircraft, explained. https://tinyurl.com/2dn3lzqs, March 2021. Accessed: 2021-03-29.

[41] James L. Felder. Nasa n3-x with turboelectric distributed propulsion. Accessed: 19.07.2024.

[42] Tobias Graf, Robin Fonk, Christiane Bauer, Josef Kallo, and Caroline Willich. Optimal Sizing of Fuel Cell and Battery in a Direct-Hybrid for Electric Aircraft. *Aerospace*, 11(3), 2024. DOI: 10.3390/aerospace11030176.

[43] Daniel Akinyele, Olabode Elijah, and Abraham Amole. Review of Fuel Cell Technologies and Applications for Sustainable Microgrid Systems. 5:1–35, 08 2020. DOI: 10.3390/inventions5030042.

[44] Omar Z. Sharaf and Mehmet F. Orhan. An overview of fuel cell technology: Fundamentals and applications. *Renewable and Sustainable Energy Reviews*, 32:810–853, 2014. DOI: https://doi.org/10.1016/j.rser.2014.01.012.

[45] Shyam S. Kocha. *Polymer Electrolyte Membrane (PEM) Fuel Cells, Automotive Applications*, pages 1–38. Springer New York, New York, NY. ISBN: 978-1-4939-2493-6. 2018. DOI: 10.1007/978-1-4939-2493-6$_{1}51 - 3$.

[46] Tabbi Wilberforce, A.G. Olabi, Imran Muhammad, Abed Alaswad, Enas Taha Sayed, Ahmed G. Abo-Khalil, Hussein M. Maghrabie, Khaled Elsaid, and Mohammad Ali Abdelkareem. Recovery of waste heat from proton exchange membrane fuel cells – A review. *International Journal of Hydrogen Energy*, 52:933–972, 2024. DOI: https://doi.org/10.1016/j.ijhydene.2022.08.069.

[47] Maria Chiara Massaro, Roberta Biga, Artem Kolisnichenko, Paolo Marocco, Alessandro Hugo Antonio Monteverde, and Massimo Santarelli. Potential and technical challenges of on-board hydrogen storage technologies coupled with fuel cell systems for aircraft electrification. *Journal of Power Sources*, 555:232397, 2023. DOI: https://doi.org/10.1016/j.jpowsour.2022.232397.

[48] Marc Schmelcher and Jannik Häßy. Hydrogen fuel cells for aviation? A potential analysis comparing different thrust categories. In *ISABE 2022*, September 2022.

[49] AVL and Red Bull Advanced Technologies. AVL and Red Bull Advanced Technologies Join Forces to Develop High Power Density Fuel Cell Technology, 2024. Accessed: 2024-07-05.

[50] Fan Zhang, Pengcheng Zhao, Meng Niu, and Jon Maddy. The survey of key technologies in hydrogen energy storage. *International Journal of Hydrogen Energy*, 41(33):14535–14552, 2016. DOI: https://doi.org/10.1016/j.ijhydene.2016.05.293.

[51] Carla Coppola, Iogann Tolbatov, Ionut Tranca, Cecilia Coletti, Alessandro Marrone, Loriano Storchi, Pietro Di Profio, Nazzareno Re, Mher Kazandjian, Antonello Pellecchia, Savino Longo, Silvia Nedea, Victor Fernandez Villace, and José Longo. A database approach for materials selection for hydrogen storage in aerospace technology. *Rendiconti Lincei. Scienze Fisiche e Naturali*, 30:287–296, 05 2019. DOI: 10.1007/s12210-019-00805-9.

[52] Etienne Rivard, Michel Trudeau, and Karim Zaghib. Hydrogen Storage for Mobility: A Review. *Materials*, 12:1973, 06 2019. DOI: 10.3390/ma12121973.

[53] Arturo Gomez and Howard Smith. Liquid hydrogen fuel tanks for commercial aviation: Structural sizing and stress analysis. *Aerospace Science and Technology*, 95:105438, 09 2019. DOI: 10.1016/j.ast.2019.105438.

[54] Nobuyuki Imanishi and Osamu Yamamoto. Rechargeable lithium–air batteries: characteristics and prospects. *Materials Today*, 17(1):24–30, 2014. DOI: https://doi.org/10.1016/j.mattod.2013.12.004.

[55] Airbus. Airbus EcoPulse. Internet, 2022.

[56] Patrick C. Vratny. Conceptual Design Methods of Electric Power Architectures for Hybrid Energy Aircraft, 2019.

[57] IEA Technology Collaboration Programme on Advanced Fuel Cells. Technology readiness level (trl) - 2023, 2023. Hydrogen fuel cell electric vehicle, High temperature proton exchange membrane, Shipping, Vehicle/aircraft/vessel and components, Transport sector, Demand.

[58] Ewa C.E. Rönnebro. Technology and manufacturing readiness of early market motive and non-motive hydrogen storage technologies for fuel cell applications. Technical report, Pacific Northwest National Laboratory, Richland, Washington 99352, June 2012. Prepared for the U.S. Department of Energy under Contract DE-AC05-76RL01830.

[59] Fabian Peter Florian Troeltsch Alejandro Castillo Pardo Biagio Della Corte Martijn van Sluis Zdobyslaw Goraj Mariusz Kowalski Xin Zhao Tomas Grönstedt Julian Bijewitz Arne Seitz, Anaïs Luisa Habermann and Guido Wortmann. Proof of concept study for fuselage boundary layer ingesting propulsion. Technical report, MDPI, 2021. DOI: https://doi.org/10.3390/aerospace 8010016.

[60] euronews. Flugzeugbau - nachhaltig leicht. https://de.euronews.com/next/2018/04/30/flugzeugbau-nachhaltig-leicht, 2018. Accessed 21.07.2024.

[61] Daniel P. Raymer. Aircraft Design: A Conceptual Approach, 1989.

[62] M. Schmidt, M. Engelmann, R. Rothfeld, M. Hornung. BOARDING PROCESS ASSESSMENT OF NOVEL AIRCRAFT CABIN CONCEPTS. https://www.icas.org/ICAS_ARCHIVE/ICAS2016/data/papers/2016_0218_paper.pdf, 2016.

[63] Graham Warwick. Aviation Promising Early Market For Advanced Battery Makers , October 2021. Accessed: 08.07.2024.

[64] Embraer. AIRPORT PLANNING MANUAL. https://www.embraercommercialaviation.com/wp-content/uploads/2017/02/APM_E175.pdf. Accessed: 21.07.2024.

[65] Simple Flying. Taxi Speeds: The Rules, Procedures Practices That Influence Taxiing. https://simpleflying.com/taxi-speeds-guide/. Accessed: 21.07.2024.

[66] DUNLOP AIRCRAFT TYRES. Reifen für Bombardier (De Havilland) Dash 8 400. https://www.dunlopaircrafttyres.co.uk/aircraft/bombardier-dash-8-400-tires/. Accessed: 20.07.2024.

[67] De Havilland Aircraft of Canada Limited. DASH 8-400. Brochure, 2023.

[68] Aircraft commerce. Dash 8 Q400 fuel burn performance. https://www.aircraft-commerce.com/wp-content/uploads/aircraft-commerce-docs/Aircraft%20guides/DASH%208%20&%20Q%20SERIES/ISSUE63_DASH8FUEL.pdf, April/May 2009.

[69] Ishwar Kanwar Puri Kalyan Annamalai. *Combustion science and engineering*. CRC Press/Taylor Francis, Boca Raton, 2007. ISBN: 9780849320712.

[70] J. Hoelzen, D. Silberhorn, T. Zill, B. Bensmann, and R. Hanke-Rauschenbach. Hydrogen-powered aviation and its reliance on green hydrogen infrastructure – Review and research gaps. *International Journal of Hydrogen Energy*, 47(5):3108–3130, 2022. Hydrogen Energy and Fuel Cells. DOI: https://doi.org/10.1016/j.ijhydene.2021.10.239.

[71] Thorbeck J. Doc-assessment method. https://www.fzt.haw-hamburg.de/pers/Scholz/Aero/TU-Berlin_DOC-Method_with_remarks_13-09-19.pdf, 2013. Accessed 21.07.2024.

[72] Kimoto B Marsh D. Beltramo M, Trapp D. *Parametric study of transport aircraft systems cost and weight*. NASA, 1977.

[73] Schäfer K. Schültke F. Risse, K. and E. Stumpf. Central reference aircraft data system (ceras) for research community. In *CEAS Aeronautical Journal 7(1), pp. 121–133*, 2016. DOI: 10.1007/s13272-015-0177-9.

[74] Clean Aviation Joint Undertaking. Strategic research and innovation agenda. Technical report, European Union, 2021.

[75] International Civil Aviation Organization. An approach to new operational concepts involving extended minimum crew operations and single-pilot operations. https://www.icao.int/Meetings/a41/Documents/WP/wp_101_en.pdf, 2022. Accessed 21.07.2024.

[76] McKinsey and Company. Hydrogen-powered aviation: A fact-based study of hydrogen technology, economics, and climate impact by 2050, May 2020.